

1 **Sources of organic aerosols in eastern China: A modeling study**
2 **with high-resolution intermediate-volatility and semi-volatile**
3 **organic compound emissions**

4 Jingyu An¹, Cheng Huang^{1*}, Dandan Huang¹, Momei Qin^{2,1}, Huan Liu³, Rusha Yan¹, Liping
5 Qiao¹, Min Zhou¹, Yingjie Li¹, Shuhui Zhu¹, Qian Wang¹, Hongli Wang¹

6 1. State Environmental Protection Key Laboratory of the Formation and Prevention of Urban Air
7 Pollution Complex, Shanghai Academy of Environmental Sciences, Shanghai 200233, China

8 2. Jiangsu Key Laboratory of Atmospheric Environment Monitoring and Pollution Control,
9 Collaborative Innovation Center of Atmospheric Environment and Equipment Technology,
10 Nanjing University of Information Science & Technology, Nanjing 210044, China

11 3. State Key Joint Laboratory of Environment Simulation and Pollution Control, School of
12 Environment, Tsinghua University, Beijing 100084, China

13 **Abstract:** ~~Organic aerosol (OA) makes up a substantial fraction of atmospheric~~
14 ~~particulate matter that exerts tremendous impacts on air quality, climate, and human~~
15 ~~health. Yet e~~Current chemical transport models fail to reproduce both the concentrations
16 and temporal variations of ~~Organic aerosol (OA)~~OA, especially the secondary organic
17 aerosol (SOA), hindering the identification of major contribution sources. ~~The absence~~
18 ~~of precursors, especially One possibility is that precursors that are not yet included in~~
19 ~~the model exist, and~~ intermediate-volatility and semi-volatile organic compounds
20 (I/SVOCs), ~~has a significant impact on the performance of SOA simulation. are~~
21 ~~advocated to be one of them.~~ Herein, we established a high-resolution emission
22 inventory of I/SVOCs and by incorporating it into the CMAQ model, concentrations,
23 temporal variations, and spatial distributions of POA and SOA originated from different
24 sources in the Yangtze River Delta (YRD) region of China were simulated. ~~By~~
25 ~~incorporating I/SVOC emissions into the model, the modeled average SOA~~

* Correspondence to C. Huang (huangc@saes.sh.cn)

26 ~~concentrations in the region increased by 148%. S~~Compared with the comprehensive
27 ~~observation data obtained in the region, i.e., volatile organic compounds (VOCs),~~
28 ~~organic carbon (OC), primary organic aerosol (POA) and SOA,~~ significant model
29 improvements in the simulations of different OA components were demonstrated by
30 comparing with the comprehensive observation data. Furthermore, spatial and seasonal
31 variations of different source contributions to OA production were identified. We found
32 cooking emissions are predominant sources of POA in the densely populated urban area
33 of the region. I/SVOC emissions from industrial sources are dominant contributors to
34 the SOA formation, followed by those from mobile sources. ~~While the former~~
35 ~~concentrated in eastern, central, and northern YRD, the latter mainly focused on the~~
36 ~~urban area.~~ Our results indicate that future control measures should be specifically
37 tailored on intraregional scale based on the different source characteristics to achieve
38 the national goal of continuous improvement in air quality. In addition, local source
39 profiles and emission factors of I/SVOCs as well as SOA formation mechanisms in
40 model framework are urgently needed to be updated to further improve the model
41 performance and thus the accuracy of source identifications.

42 **Key words:** semi-volatile and intermediate volatility organic compounds; secondary
43 organic aerosol; emission inventory; source contribution; model simulation

44 **1. Introduction**

45 Organic aerosol (OA) contributes a large fraction (20 to 90%) of atmospheric
46 submicron aerosol (Zhang et al., 2007; Jimenez et al., 2009) and has negative impacts
47 on air quality, climate (Shrivastava et al., 2017), and human health (Nault et al., 2021).
48 OA is composed of primary organic aerosol (POA) directly emitted from fossil fuel
49 combustion, biomass burning, and other sources, as well as secondary organic aerosol
50 (SOA) formed through the atmospheric oxidation of gas-phase species emitted from a
51 wide range of biogenic and anthropogenic sources (Hallquist et al., 2009).
52 Understanding and identifying the origins of OA is therefore important for elucidating
53 their health and climate effects and establishing effective mitigation policies. However,

54 OA is a dynamic system driven by the gas-particle partitioning of organic vapors and
55 particulate organic material, ~~i.e. POA and SOA~~, and continuously evolves upon
56 atmospheric oxidation (Robinson et al., 2007; Donahue et al., 2009; Zhao et al., 2013;
57 Jathar et al., 2014). It is challenging to constrain the abundance of OA precursors and
58 to identify key sources.

59 Great efforts have been made in the identification of OA sources through source
60 apportionment of the measured OA components, such as positive matrix factorization
61 (PMF) (Zhang et al., 2011), chemical mass balance (CMB) model (Zheng et al., 2002)
62 or multilinear engine (ME-2) (Canonaco et al., 2013). The Aerodyne high-resolution
63 time-of-flight aerosol mass spectrometer (AMS), has been proven to be a powerful tool
64 in quantification and chemical characterization of different OA components in real-time
65 (Canagaratna et al., 2007). Coupled with PMF analysis, AMS measurements allow for
66 the deconvolution of physically meaningful OA factors. Commonly retrieved factors
67 include three POA sources, i.e. hydrocarbon-like OA (HOA) related to fossil fuel
68 combustion, biomass burning OA (BBOA), and cooking-related OA (COA), as well as
69 two SOA components, i.e. less oxidized oxygenated OA (LO-OOA) and more oxidized
70 oxygenated OA (MO-OOA) (Hayes et al., 2013; Crippa et al., 2014; Sun et al., 2014;
71 Li et al., 2017). Combining offline AMS and radiocarbon (¹⁴C) measurements, Huang
72 et al. (2014) also identified the contributions of fossil and non-fossil sources to SOA.
73 Attempts have been made in subsequent studies by coupling the AMS measurement
74 with a suite of comprehensive and collocated SOA tracer measurements to distinguish
75 biogenic and major anthropogenic SOA sources, such as traffic and cooking emissions
76 (Xu et al., 2015; Zhang et al., 2018; Zhu et al., 2020; Huang et al., 2021a). However,
77 given the hard ionization in the AMS, there are limits to how much source information
78 can be extracted from AMS data. ~~Due to the complex OA composition and variety of~~
79 ~~emission sources~~, further deconvolution on the contributions of different sources to OA
80 production is challenging.

81 Besides field measurements, air quality modeling is another widespread technique,

82 which has advantages for regional-scale OA source apportionment with higher temporal
83 and spatial resolution. However, the model simulated SOA concentration still has large
84 gaps with that measured in the atmosphere. The volatility basis set (VBS) scheme is
85 therefore developed, which lumps organic precursors as well as their oxidation products
86 into different volatility bins. Upon atmospheric aging, the volatility of these compounds
87 evolves due to the processes such as functionalization and fragmentation, which can be
88 accounted for in the models by shifting the volatility bins of these compounds (Donahue
89 et al., 2006). Previous studies have successively configured the VBS scheme from one-
90 dimensional (1-D) to 1.5-/2-dimensions (1.5-/2-D), which can better describe the
91 evolution of OA in the 2-D space of oxidation and volatility in the model, and coupled
92 the simplified emission inventory of SOA precursors estimated from POA to improve
93 the model performance on SOA simulation~~It has been widely reported that coupling~~
94 ~~VBS scheme with air quality models can improve the model performance on SOA~~
95 ~~simulation~~ (Tsimpidi et al., 2010; Koo et al., 2014; woody et al., 2016; Zhao et al.,
96 2016a; Yang et al., 2019). However, there are still some shortcomings in the modeling
97 of OA ~~with the VBS~~, for example the lack of representation of the hydrophilic properties
98 of OA, which assumes SOA condenses onto an organic phase, whereas SOA may also
99 condense on an aqueous phase (Kim et al., 2011). Another important constraint is the
100 underestimation of intermediate-volatility organic compounds (IVOCs) and semi-
101 volatile organic compounds (SVOCs) emissions in the models, which potentially have
102 substantial contributions to SOA budget owing to their high SOA yields (Presto et al.,
103 2009; Tkacik et al., 2012; Zhao et al., 2014; Liggio et al., 2016). IVOCs refer to organic
104 compounds with effective saturation concentrations (C^*) between 10^3 to $10^6 \mu\text{g}\cdot\text{m}^{-3}$ at
105 298 K and 1 atm, while SVOCs refer to organic compounds with C^* between 10^{-1} to
106 $10^3 \mu\text{g}\cdot\text{m}^{-3}$ at 298 K and 1 atm (Robinson et al., 2007).

107 I/SVOC emission inventories have been developed and applied into air quality
108 models over the past decade. Most of them were estimated by applying different scaling
109 factors based on their relationship with POA, volatile organic compounds (VOCs), or

110 some proxies like naphthalene (Pye and Seinfeld, 2010; Shrivastava et al., 2011; Jathar
111 et al., 2017; Wu et al., 2019, 2021; Li et al., 2020, 2022; Ling et al., 2022). Yet in
112 practice, a same scaling factor was applied to most of the sources in previous studies
113 due to the lack of measurements on I/SVOC emission factors. For example, except
114 biomass burning (0.75–1.5), Wu et al. (2019) utilized scaling factors of 8–30 for all of
115 the other emission source categories, which was estimated based on the measurements
116 of on-road mobile source. Li et al. (2020) assumed scaling factors of 1.5 for on-road
117 mobile source, and 0.34–1.5 for the other sources, such as industrial and residential
118 sources, which were much lower than the estimations in Wu et al. (2020). Huang et al.
119 (2021**b**) have tried emission factor method to quantify the I/SVOC emissions, yet the
120 results were 60% lower than the scaling factor method, far from ~~catching-reproducing~~
121 the measured amount of SOA. Obviously, roughly estimating I/SVOC emissions using
122 one or two emission profiles as surrogates for all emission sources will create large
123 uncertainties.

124 Recent studies have successively determined the volatility distribution, chemical
125 composition, and emission factors of I/SVOCs from mobile sources, including gasoline
126 and diesel vehicles, non-road diesel machinery, marine vessel, and aircraft (Presto et al.,
127 2011; Cross et al., 2013; Zhao et al., 2015, 2016b; Huang et al., 2018; Qi et al., 2019;
128 Drozd et al., 2019). I/SVOC emission profiles have been reported for nonmobile-
129 sources as well, including coal combustion, wood-burning, cooking, fuel evaporation,
130 and industrial and residential volatile chemical products (Huffman et al., 2009; Gentner
131 et al., 2012; May et al., 2013; Koss et al., 2018; McDonald et al., 2018; Cai et al., 2019;
132 Drozd et al., 2021), making the quantification of I/SVOC emissions and their
133 involvement in air quality models possible.

134 In China, SOA has been emerging as an important contributor to air pollution.
135 Field observations reveal that OA contributes significantly (30%) to the PM_{2.5}
136 concentrations in most parts of China (Tao et al., 2017; Liu et al., 2018b), among which
137 the SOA contributes up to 80% of OA during haze pollution (Huang et al., 2014; Ming

138 et al., 2017; Li et al., 2021). SOA formation in China has already been examined in
139 several modeling studies. They found that by considering the POA aging and I/SVOCs
140 oxidation in the models, which is realized by the coupling of VBS scheme, the
141 formation and evolution of SOA can be much better simulated compared to the results
142 of the two-product SOA modeling framework (Zhao et al., 2016a; Wu et al., 2019; Li
143 et al., 2020; Yao et al., 2020; Huang et al., 2021**b**). Chang et al. (2022) developed a full-
144 volatility organic emission inventory with source-specific I/SVOC emission profiles for
145 China, which have greatly improved the model performance on SOA concentrations.
146 However, large gaps still exist between the observed and modeled SOA. Studies on
147 high-resolution I/SVOC emission inventory for more specific sources are highly needed.

148 In this study, taking the Yangtze River Delta (YRD) region, including Jiangsu,
149 Zhejiang, Anhui provinces and Shanghai city, as a pilot, we established a high-
150 resolution source specific I/SVOC emission inventory. We then applied the established
151 inventory into CMAQ v5.3 to evaluate the contributions of I/SVOC emissions to SOA
152 formation by comparing the results with the observation data collected in the region.
153 Furthermore, we also run the model in different scenarios to quantify the seasonal
154 contributions of different sources to POA and SOA formation in the YRD region.

155 **2. Materials and methods**

156 2.1 I/SVOC emission inventory

157 ~~I/SVOCs commonly exist in both gas and particle phase in the atmosphere.~~
158 Previous studies usually used POA scaling factors to estimate the I/SVOC emissions,
159 which may lead to large uncertainties in the estimation of gas-phase organic compound-
160 dominated sources, like oil refinery, chemical production, and industrial solvent-use.
161 Herein, we compiled both gas-phase ~~I/SVOCs (I/SVOCs-G)~~ and particle-phase
162 ~~I/SVOCs (I/SVOCs-P)~~ emission inventories and incorporate them into the model.
163 Detailed process of the inventories is as follows.

164 (1) Source classification: To refine the I/SVOC emissions from different sources,
165 we divided the sources into five major categories and then further grouped them into

166 21 sub-categories. The major categories include industrial process sources, industrial
167 solvent-use sources, mobile sources, residential sources, and agricultural sources. As
168 shown in Table S1, the industrial process sources include the sectors such as oil refinery,
169 chemical production, and pulp and paper production; Industrial solvent-use sources
170 include textile, leather tanning, timber processing, and various industrial volatile
171 chemical products use; Mobile sources include gasoline and diesel vehicle emissions,
172 fuel evaporation, diesel machinery, marine vessel, and aircraft; Residential sources
173 include coal combustion, residential solvent-use, and cooking emissions; Agricultural
174 source is specifically referred to biomass burning in household stoves, and open burning
175 was not included in this study.

176 (2) Emission estimation: ~~I/SVOCs-G~~Gas-phase emissions for each specific source
177 were estimated by the ratios of total I/SVOC components to anthropogenic VOC
178 (AVOC) components (~~I/SVOCs-to-G-ratio~~VOCs). Similarly, ~~I/SVOCs-P~~particle-phase
179 emissions were estimated by the ratios of total particle-phase I/SVOC components to
180 POA (~~I/SVOCs-to-P-ratio~~POA). The ~~I/SVOCs-G-to-VOCs~~ and ~~I/SVOCs-P-to-POA~~
181 ratios for each source were determined according to their fractions of total I/SVOC
182 species in VOC and POA emissions. Then we grouped different I/SVOC species into
183 lumped I/SVOC bins based on their C^* to determine the volatility distributions of each
184 source. The ~~I/SVOCs-G~~gas-phase emissions were distributed into four lumped aliphatic
185 IVOC bins across the volatility basis set from $C^*=10^3$ to $10^6 \mu\text{g}\cdot\text{m}^{-3}$, two aromatic
186 IVOC bins with the $C^*=10^5$ and $10^6 \mu\text{g}\cdot\text{m}^{-3}$, and four lumped SVOC bins with C^* from
187 10^{-1} and $10^2 \mu\text{g}\cdot\text{m}^{-3}$. The ~~I/SVOCs-P~~particle-phase emissions were distributed into five
188 bins spanning C^* from 10^{-1} and $10^3 \mu\text{g}\cdot\text{m}^{-3}$. Source profiles of I/SVOC species for
189 different sources were referenced from the results in previous studies. Table S1 and S2
190 show the ~~I/SVOCs-G-to-VOCs-ratios~~ and ~~I/SVOCs-P-to-POA~~ratios for each specific
191 source and their references. For industrial process, industrial solvent-use, and
192 residential solvent-use sources, only ~~I/SVOCs-G~~gas-phase emissions were considered.
193 Their ~~I/SVOCs-G-to-VOCs-G~~ratios and emission profiles were derived from the latest

194 version of SPECIATE 5.1 database (US EPA, 2021). For gasoline and diesel vehicles,
195 the ~~I/SVOCs-G-to-VOCs-G-ratios~~ and ~~I/SVOCs-P-to-POA-P-ratios~~ and emission
196 profiles were referenced from a new mobile-source parameterization recommended by
197 Lu et al. (2020). Those of diesel machinery, marine vessel, and residential coal
198 combustion were determined by recent measurement results in China (Qi et al., 2019;
199 Huang et al., 2018; Cai et al., 2019). The ~~I/SVOCs-G-to-VOCs-G-ratios~~ and profiles of
200 cooking and biomass burning emissions were derived from SPECIATE 5.1 database,
201 while their ~~particle-phase-P-ratios~~ and profiles were referenced from two previous
202 studies (May et al., 2013; Louvaris et al., 2017). ~~Table S1 and S2 show the I/SVOCs-~~
203 ~~G-to-VOCs and I/SVOCs-P-to-POA ratios and their emission profiles of each specific~~
204 ~~source~~. The base emissions of AVOCs and POA (See Table S3) were taken from a high-
205 resolution emission inventory for the year of 2017 developed in our previous study (An
206 et al., 2021).

207 (3) Model input: Before being input into the model, the estimated ~~I/SVOC-Ggas-~~
208 ~~phase~~ and ~~I/SVOC-Particle-phase~~ emissions were summed and then redistributed
209 according to their phase equilibrium under the actual atmospheric state. The formula of
210 phase equilibrium is shown in Equation (1).

$$211 \quad F_p = \frac{C_{OA}}{C_{OA} + C^*} \quad (1)$$

212 Where, F_p is the fraction of particle-phase ~~I/SVOC~~ emissions for each volatility bin.
213 C_{OA} represents the OA concentration in the atmosphere. We assumed it to be $10 \mu\text{g}\cdot\text{m}^{-3}$
214 in this study. C^* is the effective saturation concentration of each volatility bin. After
215 redistribution, the I/SVOC emissions for each source category were allocated into 4 km
216 $\times 4 \text{ km}$ grids and hourly temporal profiles using the same method as the criteria
217 pollutants.

218 2.2 Model configuration

219 We used Community Modeling and Analysis System (CMAQ version 5.3.2) to
220 simulate the concentrations of air pollutants. The domain of the simulation is presented
221 in Figure 1. The simulations were conducted for three nested grids with horizontal

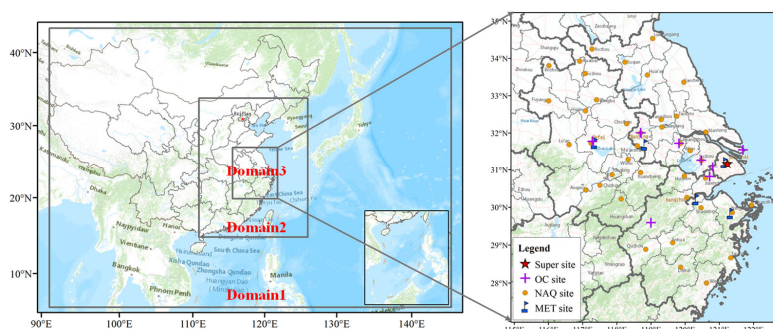
222 resolution of 36 km (D1), 12 km (D2) and 4 km (D3), respectively. D1 covers most of
223 China and the surrounding countries including Japan and South Korea; D2 covers
224 eastern China and D3 covers the entire YRD region and its surrounding land and waters.

225 Meteorological fields were provided by the Weather Research and Forecasting
226 (WRF version 3.7) model with 27 vertical layers extending to the tropopause (100 hpa).
227 The initial and boundary conditions (ICs, BCs) in the WRF were based on the $1^\circ \times 1^\circ$
228 reanalysis data from the National Centers for Environmental Prediction Final Analysis
229 (NCEP-FNL). Physical options used in the WRF simulation are listed in Table S4.

230 The Sparse Matrix Operator Kernel Emissions (SMOKE,
231 <https://cmasceneter.org/smoke>) model was applied to process emissions for input to
232 CMAQ. CMAQ version 5.3.2 (<https://cmasceneter.org/cmaq/>) was used to simulate
233 atmospheric pollutants concentrations. ICs and BCs of D1 domain are based on a Model
234 For Ozone And Related Chemical Tracers (MOZART) global simulation
235 (<https://acom.ucar.edu/wrf-chem/mozart.shtml>). For the inner D2 and D3 domain, ICs
236 and BCs are extracted from the simulation results of the outer domains. Options selected
237 for the CMAQ simulations include the SAPRC07 gas phase chemistry, the AERO7
238 aerosol scheme, the Regional Acid Deposition Model (RADM) model aqueous phase
239 chemistry, [and](#) ISORROPIA inorganic particulate thermodynamics.

240 The emission inventory developed in this study was used to produce the emission
241 system in the YRD region while emissions beyond YRD were supplied by
242 Multiresolution Emission Inventory for China (MEIC-2017, <http://meicmodel.org>),
243 Shipping Emission Inventory Model (SEIM) (Liu et al., 2016), and the Model Inter-
244 Comparison Study (MIX) emission inventory for 2010 (Li et al., 2017). The I/SVOC
245 emission inventory outside the YRD region was developed by multiplying the VOCs
246 and POA emissions with the average ~~I/SVOCs-G-to-VOCsG-ratios~~ and ~~I/SVOCs-P-~~
247 ~~to-POA-P-ratios~~ of major source categories like industry, vehicle, marine vessel, and
248 residential. Biogenic volatile organic compounds (BVOCs) emissions were estimated
249 based on MEGAN (the Model of Emissions of Gases and Aerosols from Nature) version

250 2.10 driving by inputs of the leaf area index (LAI) from MODIS product, plant
251 functional types (PFT) base on remote sensing data, inline coupled emission factors and
252 meteorology simulated by the WRF model. Detail configurations of MEGAN can be
253 obtained from our previous study (Liu et al., 2018a).



254
255 **Figure 1.** Modeling domain and locations of observation sites. The blue marks are meteorological
256 monitoring sites. The yellow dots represent the national air quality monitoring sites. The purple
257 crosses are the observation sites with PM_{2.5} chemical composition measurements. The red star
258 represents the observation site of AMS measurement.

259 SOA formed from I/SVOCs was estimated using the parameterization within the
260 VBS framework in Lu et al. (2020). Specifically, the I/SVOC surrogates react with OH,
261 generating four oxygenated organic species with volatility spanning from $C^* = 10^{-1}$ to
262 $10^2 \mu\text{g}\cdot\text{m}^{-3}$, which may exist in both gas and condensed phase. The rate coefficient (i.e.,
263 k_{OH}) and product yields (i.e., α_i , $i=1, 2, 3, 4$) for each primary I/SVOC species were
264 derived based on previous laboratory results (Zhao et al., 2015; Zhao et al., 2016b).
265 Multi-generation oxidation was considered by implementing further oxidation of the
266 vapors from the initial oxidation, which redistributes the mass across the volatility bins
267 of $C^* = 10^{-2}$ to $10^2 \mu\text{g}\cdot\text{m}^{-3}$, and thus fragmentation and functionalization were included.
268 It is worth noting that only one-step oxidation of the vapor products was considered,
269 using the default aging scheme for the oxidation products of POA in the CMAQ
270 (Murphy et al., 2017). Additionally, SOA formation from SVOCs were treated similarly,
271 and more details can be found in Murphy et al. (2017). POA was treated as semivolatile

272 to account for its gas-particle partitioning and ageing process and segregated to several
 273 particle species, which varied in their volatility that quantified with the metric $C^* = 10^{-1}$
 274 1 to $10^3 \mu\text{g}\cdot\text{m}^{-3}$ (Donahue et al., 2006). ~~I/SVOCs-PParticle-phase~~ emissions from
 275 different sources were then speciated and input as semivolatile accordingly. The
 276 remaining POA emissions excluding ~~I/SVOCs-Particle-phase I/SVOCs~~ were treated
 277 as nonvolatile POC (primary organic carbon) and PNCOM (primary non-carbon
 278 organic matter).

279 2.3 Model simulations

280 To investigate the model performance on OA simulations and the contributions of
 281 different sources, we set 14 simulation cases using brute-force method (Zhang et al.,
 282 2005). Table 1 shows the settings for these 14 cases. First was BASE simulation case,
 283 in which the I/SVOC emissions was not included and the POA emissions were treated
 284 as non-volatile. The second was the ~~IMPROVE-I/SVOC-E~~ case, which augmented the
 285 high-resolution I/SVOC emission inventory established in this study. In addition, the
 286 POA emissions in the ~~I/SVOC-EIMPROVE~~ simulation were split into both non-volatile
 287 and semivolatile parts. The non-volatile emissions were obtained by subtracting the
 288 ~~I/SVOCs-PP-ratios~~ from the total POA. The semivolatile emissions, that was ~~I/SVOCs-~~
 289 ~~Pparticle-phase-emissions~~, were treated with variable gas-particle partitioning and
 290 multigenerational aging in this simulation case. We then used the difference between
 291 ~~I/SVOC-EIMPROVE~~ and BASE cases to evaluate the OA contributions from I/SVOC
 292 emissions. CASE1 to CASE12 respectively excluded the VOC and I/SVOC emissions
 293 from different sources. We used the differences between ~~I/SVOC-EIMPROVE~~ and
 294 CASE1-12 to quantify the contribution of each source to OA concentration.

295 **Table 1.** Settings of simulation cases.

Name	Sources with added I/SVOC emissions
BASE	none
I/SVOC- EIMPROVE	all
CASE1	all except industrial process
CASE2	all except industrial solvent-use

CASE3	all except mobile sources
CASE4	all except residential sources
CASE5	all except biomass burning
CASE6	all except biogenic sources
CASE7	without VOCs and I/SVOC emissions
CASE8	all except gasoline vehicle
CASE9	all except diesel vehicle
CASE10	all except diesel machinery
CASE11	all except marine vessel
CASE12	all except cooking

296 2.4 Model evaluation

297 To capture the characteristics of OA with different meteorological features in the
 298 YRD region, we selected four periods to represent spring (Mar. 15th to Apr. 15th, 2019),
 299 summer (Jul. 1st to 31st, 2019), autumn (Oct. 15th to Nov. 15th, 2018), and winter (Dec.
 300 1st to 31st, 2018) to conduct the simulations. Evaluations on model performance were
 301 made by comparing the simulation results with the observations obtained in the region,
 302 including 5 meteorological observation sites, 10 PM_{2.5} chemical composition sites, and
 303 41 national air quality monitoring sites, one in each city. The locations of the
 304 meteorological and air pollutant observation sites are shown in Figure 1.

305 We also used the observation data of an AMS and a GC-MS/FID system at the
 306 supersite in Shanghai to further verify the model performance on the simulation of POA,
 307 SOA, and key VOC precursors. Details of AMS measurements and PMF analysis are
 308 provided in our previous study (Huang et al., 2021a). A total of 55 PAMS
 309 (Photochemical Assessment Monitoring Stations) species were identified by the GC-
 310 MS/FID system including 27 alkanes, 11 alkenes, acetylene and 16 aromatics. The
 311 supersite was located on the top-floor of an eight-story building in Shanghai Academy
 312 of Environmental Sciences (SAES, 31°10' N, 121°25'E), 30 m above the ground. The
 313 site was in a typical residential and commercial area with significant influence from
 314 traffic emission. Several petrochemical and chemical industrial factories sit around 50
 315 km away from the site to the south and southwest.

316 Model performance in simulation of meteorological parameters and major criteria

317 air pollutants are summarized in Table S5 and S6. The mean bias (MB), mean gross
318 error (MGE), root-mean-square error (RMSE), and index of agreement (IOA) of
319 temperature, humidity, wind speed, and wind direction in each season are within the
320 criteria recommended by Emery et al. (2001). Although the temperature in summer and
321 winter, and wind speed in autumn and winter were slightly overestimated, their MGE
322 and IOA values are within the uncertainties as recommended in Emery et al. (2001).

323 For the simulation of major criteria air pollutants, both mean fractional bias (MFB)
324 and mean fractional error (MFE) of all pollutants met the criteria recommended by
325 Boylan and Russell (2006). Since the addition of I/SVOC emissions would change the
326 PM_{2.5} simulation results, we thus presented the statistical results for both BASE and
327 ~~IMPROVE-I/SVOC-E~~ cases in the Table S6. ~~The simulated SO₂ was slightly~~
328 ~~overestimated, which might be caused by the overestimation of SO₂ emissions due to~~
329 ~~the fact that China's SO₂ emission reduction was far beyond the expectation. The~~
330 ~~modeled SO₂ was slightly overestimated, which is likely due to the faster than expected~~
331 ~~reduction of SO₂ emissions, resulting in overestimation of SO₂ emissions in the~~
332 ~~emission inventory. On the~~ contrast, the modeled NO₂ were underestimated in
333 spring, autumn, and winter, likely due to the overestimation of wind speed in these
334 seasons. The modeled O₃ and PM_{2.5} were slightly overestimated in the ~~I/SVOC-~~
335 ~~EIMPROVE~~ simulation case. Overall, the simulated meteorological parameters and
336 major criteria air pollutants are consistent with the observations.

337 3. Results and discussion

338 3.1 I/SVOC emission inventory

339 3.1.1 Source-specific I/SVOC emissions

340 Table 2 shows the ~~I/SVOCs-Ggas-phase~~ and ~~I/SVOCs-Pparticle-phase~~ emission
341 inventories for detailed source category for year 2017 in the YRD region. The total
342 ~~I/SVOC-Ggas-phase~~ emission in the YRD region was 1148.42 Gg in 2017, lower than
343 that in Wu et al. (2021) of 1360 Gg, but higher than the estimate in Huang et al. (2021b)

设置了格式: 下标

设置了格式: 下标

设置了格式: 下标

344 of 730 Gg. We found industrial solvent-use was the largest contributor (483.644 Gg,
345 42.14%) of total ~~I/SVOCs-Ggas-phase~~ emissions, followed by industrial process
346 sources (244.655 Gg, 21.36%), mobile source (344.31 Gg, 29.9830.0%), residential
347 source (62.23 Gg, 5.42%), and agriculture source (13.584 Gg, 1.182%). Specifically,
348 chemical production, textile, and solvent-based coating were major sectors of ~~I/SVOCs-~~
349 ~~Ggas-phase~~ emissions in the YRD region, accounting for 20.86%, 19.54%, and 15.071%
350 of the total ~~I/SVOCs-Ggas-phase~~ emission, and their contributions to AVOC emissions
351 were 20.76%, 2.22%, and 23.42%, respectively (See Table S3). The chemical materials
352 and production process of these industries were quite different, which would make their
353 G-ratios quite different in the profiles. It is interesting to note that the I/SVOCs-to-
354 VOCs ratios are largely different for different sources. For example, the textile industry
355 only accounted for 2.22% of the total AVOC emissions in the YRD region but
356 contributed to 19.54% of the ~~I/SVOC-Ggas-phase~~ emissions due to its higher ~~I/SVOCs-~~
357 ~~to-VOCs-G~~-ratio (2.473). Another example is water-based coatings, whose VOC
358 emissions were approximately 10.2% of solvent-based coatings, while their I/SVOC
359 emissions were 29.1% of those from solvent-based coatings. These findings indicate
360 that reductions in VOC emissions not necessarily corresponds to the simultaneous
361 reductions in I/SVOCs emissions and subsequent SOA formation, which should be
362 considered in future control strategies- (Yuan et al., 2010).

363
364 For ~~I/SVOCs-Ggas-phase~~ emission of mobile origin, the major contributors were
365 gasoline vehicle, diesel vehicle, and non-road diesel machinery, accounting for 13.64%,
366 11.667%, and 2.14%, respectively. The total ~~I/SVOCs-Ggas-phase~~ emissions from
367 gasoline and diesel vehicles were 290.571 Gg, much higher than the results reported in
368 Liu et al. (2017) (3029.58 Gg) and Huang et al. (2021b) (16.0 Gg) using the emission
369 factor method, which likely underestimates the emission factors of I/SVOCs due to the
370 lack of localized emission factors. Our tunnel experiment results show that the average
371 IVOcs emission factors of gasoline and diesel vehicles were 15.3 mg·km⁻¹ and 219.8

372 mg·km⁻¹ (Tang et al., 2021), which were significantly higher than those used in the
 373 above studies (Liu et al., 2017; Huang et al., 2021b). More comprehensive localized
 374 emission measurements are advocated to better constrain the I/SVOC emissions from
 375 mobile sources.

376 ~~I/SVOCs-Pparticle-phase~~ emissions were ~~82.963~~ Gg. The largest contributor of
 377 ~~I/SVOCs-Pparticle-phase~~ emissions came from cooking emission and diesel vehicle,
 378 accounting for 53.24% and 11.889% of the total, followed by gasoline vehicle (5.23%),
 379 marine vessel (2.667%), diesel machinery (2.54%), and biomass burning (1.758%).
 380 Note that the ~~I/SVOCs-Pparticle-phase~~ emissions from coal combustion (e.g. power
 381 plants, boilers, etc.), other industrial processes, and aircraft were not included in this
 382 study. On the one hand, the POA emissions (See Table S3) from these sources were
 383 limited, accounting for less than 5%, which could be expected that their ~~I/SVOCs-~~
 384 ~~Pparticle-phase~~ emissions were also relatively low. On the other hand, the profiles of
 385 ~~I/SVOCs-Pparticle-phase~~ components of these sources were still difficult to obtain.
 386 More measurements of the I/SVOC emissions from these sources is very necessary in
 387 the future.

388 **Table 2.** Source-specific emissions of I/SVOCs for the year 2017 in the YRD region.

Source	I/SVOCs		I/SVOCs-GGas- phase		I/SVOCs- Pparticle-phase		
	Gg	%	Gg	%	Gg	%	
Oil refinery	5.63	0.46	5.62	0.49	0.01	0.01	
Industrial process	243.604	19.78 8	238.912	20.80	4.69	5.65	
	Pulp and paper	0.11	0.01	0.11	0.01	0.00	0.00
Industrial solvent-use	Textile	229.7830	18.66 7	224.06	19.51	5.72	6.90
	Leather tanning	3.83	0.31	3.83	0.33	0.00	0.00
	Timber processing	31.081	2.52	31.081	2.71	0.00	0.00
	Furniture coating	1.32	0.11	1.32	0.12	0.00	0.00
	Solvent-based coating	173.02	14.05 1	173.01	15.07 1	0.00	0.00
	Water-based coating	50.32	4.09	50.32	4.38	0.01	0.01
	Dry cleaning	0.02	0.00	0.02	0.00	0.00	0.00

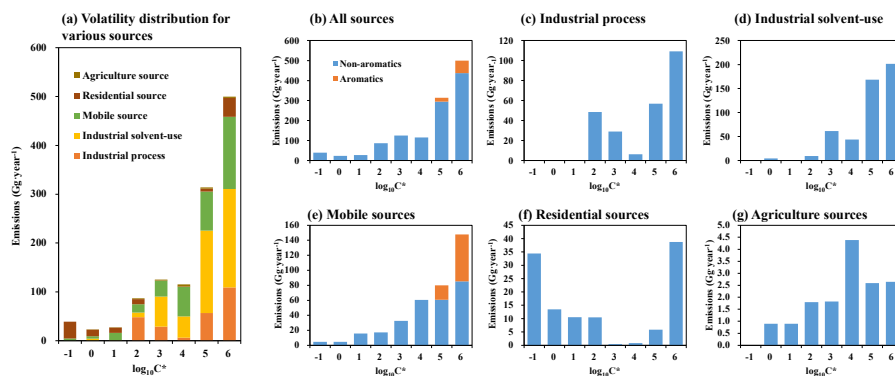
	Paint remover	0.01	0.00	0.01	0.00	0.00	0.00
Mobile source	Gasoline vehicle	161.041	13.08	156.677	13.64	4.34	5.23
	Diesel vehicle	143.764	11.67	133.904	11.66	9.86	11.88
	Fuel evaporation	0.69	0.06	0.69	0.06	0.00	0.00
	Diesel machinery	49.62	4.03	47.51	4.14	2.11	2.54
	Marine vessel	7.12	0.58	4.91	0.43	2.21	2.66
	Aircraft	0.64	0.05	0.64	0.06	0.00	0.00
	Residential source	Coal combustion	2.73	0.22	2.73	0.24	0.00
	Residential solvent-use	35.293	2.87	35.29	3.07	0.09	0.11
	Cooking	76.778	6.23	24.39	2.12	52.465	63.24
Agriculture source	Biomass burning	15.04	1.22	13.586	1.18	1.45	1.75
	Total	1231.38	100.00	1148.42	100.00	82.963.0	100.00

389 3.1.2 Volatility distributions of I/SVOCs

390 Figure 2 shows the volatility distribution of I/SVOC emissions from different
391 sources as well as their gas-particle distributions. The I/SVOC emissions generally
392 showed an increasing trend with the increase of volatility. As shown in Figure 2(a),
393 IVOC emissions (logC* bins at 3–6) accounted for 86% of the total I/SVOCs emissions,
394 overwhelmingly dominated by industrial process and mobile sources. SVOCs (logC*
395 bins at 0–2) and low-volatile organic compounds (LVOCs, logC* bins at -1) contributed
396 to 11% and 3% of the total I/SVOCs emissions. In terms of the contributing sectors,
397 mobile sources, industrial process, and solvent-use dominated the total I/SVOC
398 emissions. While the IVOCs were equally contributed by above-listed three sources,
399 residential and mobile sources dominated the SVOCs and LVOCs emissions.

400 We further investigated the contributions of different volatility bins to each source
401 category. The mobile source was dominated by IVOC emission (88%). Note that IVOC
402 emissions from vehicles included a certain fraction of aromaticsIVOCs in vehicle
403 exhaust are dominated by aromatics, which have faster OH reaction rates and higher
404 SOA yields compared to aliphatics in the same volatility bin (Zhao et al., 2016b; Drozd
405 et al., 2019). Lu et al. (2020) therefore defined two additional lumped IVOC species

406 with $\log C^*$ bins at 5 and 6 to account for the aromatic IVOCs in vehicle exhaust
 407 according to the measurements in previous studies (Zhao et al., 2015; Zhao et al.,
 408 2016b). Here in this study, we also split the aromatic IVOC emissions from mobile
 409 sources and found that aromatic IVOCs accounted for 23% of the total I/SVOC
 410 emissions from the mobile source. The industrial process and solvent-use sources were
 411 also dominated by IVOC emissions, accounting for 81% and 97%, respectively. The
 412 volatility distribution of residential sources was relatively uniform, with IVOCs,
 413 SVOCs and LVOCs accounting for 40%, 30%, and 30%. Agricultural (i.e., biomass
 414 burning) sources were more concentrated in IVOCs, accounting for 76%, while SVOCs
 415 accounted for 24%. It should be noted that other than mobile sources, the emission
 416 profiles of the other sources were mainly derived from SPECIATE 5.1 database (US
 417 EPA, 2021) in this study, which may be inconsistent with real-world emissions in China.
 418 To further reduce the uncertainty in the I/SVOC emission inventory, measurements of
 419 I/SVOC emissions from different local sources are therefore important and urgently
 420 needed in the future.



422 **Figure 2.** Volatility distributions of I/SVOCs emitted from different sources in the YRD region.

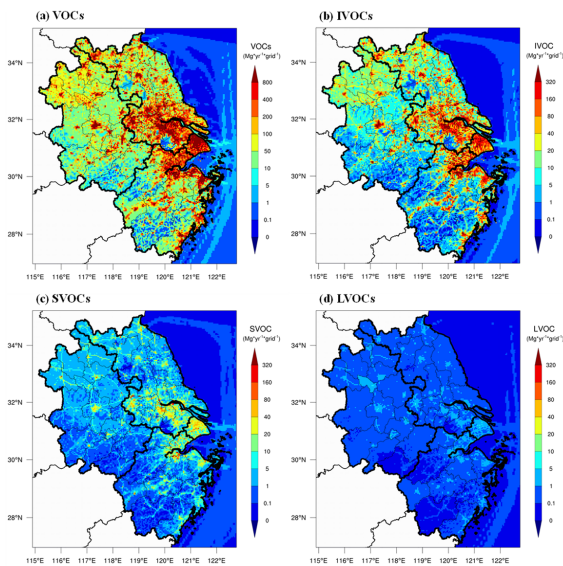
423 3.1.3 Spatial distributions of I/SVOC emissions in YRD region

424 Figure 3 compares the spatial distributions of AVOC, IVOC, SVOC, and LVOC
 425 emissions in the YRD region. The IVOC, SVOC, and LVOC emissions were largely
 426 concentrated in city clusters in eastern YRD, and hotspots can also be observed in the

427 northern agglomerations. The distributions of I/S/LVOC emissions were generally
428 consistent with that of the AVOC emissions in the region. Compared to the spatial
429 distributions of I/S/LVOC emissions in Chang et al. (2022), our emissions had similar
430 spatial distributions but at a higher resolution. Emission hotspots in urban areas can be
431 captured more clearly in this study, which will help improve the simulation in urban
432 areas.

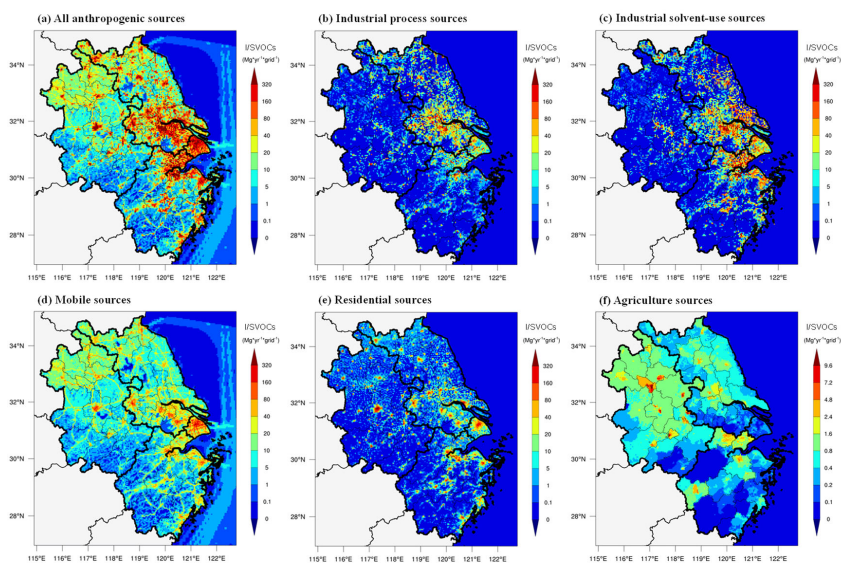
433 Figure 4 shows the spatial distributions of source-specific I/SVOC emissions in
434 the YRD region. There were considerable differences in the spatial distributions of
435 I/SVOC emissions from different sources. The I/SVOC emissions from industrial
436 sources (including industrial process and industrial solvent-use) were mainly
437 concentrated in the eastern urban agglomeration, which was related to the developed
438 industrial activities in the region. The I/SVOC emissions from mobile and residential
439 sources clustered into multiple hotspots in urban areas, while emissions from
440 agricultural sources were mainly distributed in northern YRD, where frequent
441 agricultural activities exist.

442 We also compare the spatial distributions of I/SVOC emissions with those of POA
443 and BVOCs. We found that POA emissions were more concentrated in urban centers
444 associated with mobile and residential sources (See Figure S1). BVOC emissions in the
445 YRD region were mainly distributed in the southern area, where AVOC and IVOC
446 emissions were relatively low. The difference in the spatial distributions of I/SVOC,
447 AVOC, BVOC, and POA emissions implies that the sources of organic components in
448 different areas of the region are quite different, which will be discussed in the following
449 sections.



450

451 **Figure 3.** Spatial distributions of anthropogenic VOC, IVOC, SVOC, and LVOC emissions in the
 452 YRD region for the year 2017.



453

454 **Figure 4.** Spatial distributions of I/SVOC emissions from different source categories in the YRD
 455 region for the year 2017.

456 3.2 Comparison between model simulation and observation

457 3.2.1 Simulation results of VOCs and IVOCs

458 Since model performance on the simulation of VOCs are critical for SOA
459 estimation, we first compare the modeled concentrations of VOCs with those of the
460 measured at the SAES supersite for several aromatic VOCs, including benzene, toluene,
461 and m-/p-/o-xylenes. As shown in Figure S2, the model simulation was able to capture
462 the hourly variations of these species measured, with Pearson correlation coefficients
463 (r) of 0.54–0.65, 0.45–0.60, 0.54–0.69 for toluene, xylene, and benzene respectively.
464 Although the simulation results of toluene were 28% lower and xylene and benzene
465 were 41% and 22% higher than those of the measured, the model results are within the
466 uncertainties. Overall, the simulation results of the VOC species showed good
467 agreements with the observations, which could be further used for the model simulation
468 of SOA formation.

469 Long-term continuous observations of I/SVOC concentrations were sparse, so the
470 simulation results of IVOCs were compared with those obtained from offline
471 measurements reported in our previous studies (Li et al., 2019; Ren et al., 2020). The
472 reported IVOC concentrations (sum of gas- and particle-phase concentrations) in
473 summer and winter Shanghai in 2018 respectively varied between 1.5–17.2 and
474 2.2–43.1 $\mu\text{g}\cdot\text{m}^{-3}$ with average concentrations of 6.8 ± 3.7 and $18.2 \pm 11.0 \mu\text{g}\cdot\text{m}^{-3}$. In
475 this study, our modeled average concentrations of IVOCs in spring, summer, autumn,
476 and winter at the SAES supersite in Shanghai were 12.8 ± 5.6 , 9.0 ± 3.2 , 12.2 ± 5.2 ,
477 and $12.4 \pm 7.6 \mu\text{g}\cdot\text{m}^{-3}$, respectively. The modeled IVOCs was higher in summer while
478 lower in winter. Although there was still a deviation of 20%–30% between the
479 simulation and observation, not to mention the diurnal patterns and spatial distributions
480 also remained unknown, the simulation results are at least comparable to those of the
481 measured concentrations, suggesting the modeled I/SVOCs is appropriate to be used in
482 the estimation of SOA production from different sources. This may be due to the
483 difference in monthly profiles of I/SVOC emissions, which has not been considered in

484 ~~this study. Another important reason should be the chemical mechanism of IVOCs to~~
485 ~~SOA evolution still needs to be improved.~~ Continuous long-term measurements of
486 I/SVOC at multiple locations are strongly recommended in the future to ~~help to~~ improve
487 the ~~SOA~~ model performance ~~and reduce the uncertainties in SOA estimation.~~

488 3.2.1 Simulation results of OA concentrations

489 Figure 5 presents the OA concentrations originated from different sources,
490 including POA and SOA formed from AVOCs, BVOCs, and I/SVOCs, in four seasons
491 in YRD from both BASE and ~~I/SVOC-EIMPROVE~~ simulations. Here we used the
492 average of the modeled concentrations at 41 national air quality monitoring sites (See
493 the yellow dots in Figure 1) to represent the regional average. The regional average
494 concentration of OA (~~8.75-8~~ $\mu\text{g}\cdot\text{m}^{-3}$) in the ~~I/SVOC-EIMPROVE~~ simulation was 22%
495 higher than that from BASE simulation (~~7.47-2~~ $\mu\text{g}\cdot\text{m}^{-3}$) due to the involvement of
496 I/SVOCs in the ~~I/SVOC-EIMPROVE~~ simulation.

497 The seasonal average concentration of POA was $5.5 \mu\text{g}\cdot\text{m}^{-3}$ in the BASE case, with
498 the lowest in summer ($3.8 \mu\text{g}\cdot\text{m}^{-3}$) and the highest in winter ($6.9 \mu\text{g}\cdot\text{m}^{-3}$). High POA
499 concentrations in winter was mainly induced by the stagnant meteorological conditions
500 such as low wind speed and boundary layer height ~~and weaker photochemical effect,~~
501 and vice versa in summer. For the spatial distributions as presented in Figure 6, POA
502 concentrations in northern YRD were high and mainly concentrated in urban areas,
503 which was consistent with the distributions of POA emissions (Figure S1). The POA
504 concentrations in the ~~I/SVOC-EIMPROVE~~ simulation decreased by 12%–20%
505 compared with the BASE case. In the ~~I/SVOC-EIMPROVE~~ simulation, the POA was
506 treated as semi-volatile, where gas–particle partitioning and multigeneration oxidation
507 were considered (Murphy et al., 2017). Entering into the atmosphere, more semi-
508 volatile compounds evaporated into gas-phase and then generated SOA through
509 multigeneration oxidation, which reduced the POA concentrations relatively.

510 The seasonal average concentration of AVSOA in the BASE case was only ~~0.22~~
511 $\mu\text{g}\cdot\text{m}^{-3}$. The average AVSOA concentration in the ~~I/SVOC-EIMPROVE~~ case increased

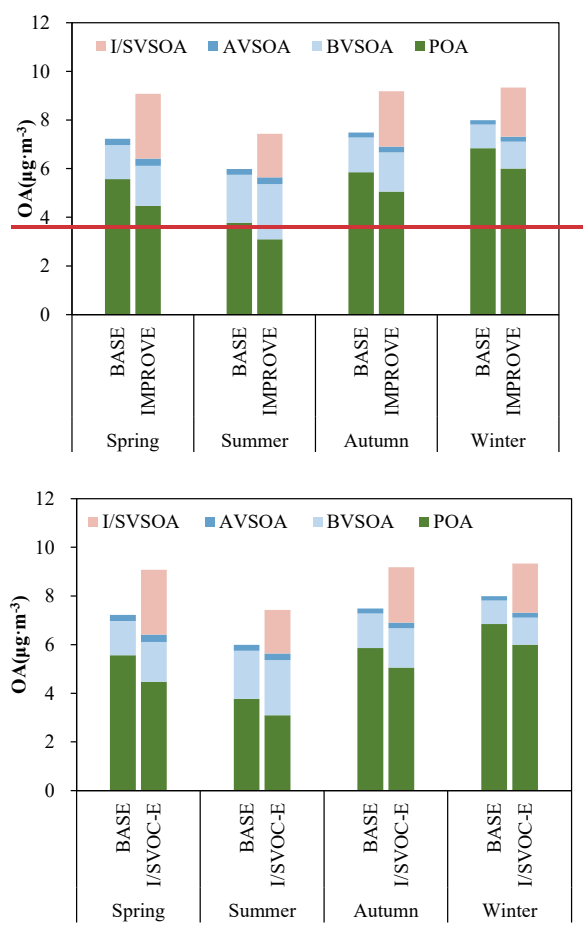
512 by 17% compared with the BASE case due to higher OA loading. Nonetheless, AVSOA
513 still exhibited very limited contribution to the regional OA concentration, whereas
514 average concentration of BVOC derived SOA (BVSOA, $1.7 \mu\text{g}\cdot\text{m}^{-3}$ in the I/SVOC-
515 EIMPROVE simulation case) was much higher. Also, evident seasonal variations were
516 observed for BVSOA, with the highest in summer ($2.27\text{-}3 \mu\text{g}\cdot\text{m}^{-3}$), followed by spring
517 ($1.65\text{-}7 \mu\text{g}\cdot\text{m}^{-3}$), autumn ($1.62 \mu\text{g}\cdot\text{m}^{-3}$), and winter ($1.14 \mu\text{g}\cdot\text{m}^{-3}$). Hotspots of BVSOA
518 concentrations were concentrated in the western and southern YRD. The observed
519 seasonal variations and spatial distributions of BVOC derived SOA were consistent
520 with those of the BVOC emissions in YRD (Liu et al., 2018a).

521 The average concentration of I/SVOC derived SOA (I/SVSOA) in I/SVOC-
522 EIMPROVE simulation was $2.48\text{-}2 \mu\text{g}\cdot\text{m}^{-3}$, with the highest in spring ($2.66\text{-}7 \mu\text{g}\cdot\text{m}^{-3}$)
523 and the lowest in summer ($1.79\text{-}8 \mu\text{g}\cdot\text{m}^{-3}$), which was a combined effect of emission,
524 oxidation and meteorological conditions. For example, Qin et al. (2022) suggested that
525 in spring the enhanced solar radiation and OH oxidation potentially promote the
526 secondary conversion from I/SVOCs to SOA. The low concentration in summer was
527 likely due to the better meteorological conditions than the other seasons. By
528 incorporating I/SVOC emissions into the I/SVOC-EIMPROVE simulation, the
529 modeled average SOA concentration in the region increased from $1.66\text{-}7$ (BASE) to
530 $4.10 \mu\text{g}\cdot\text{m}^{-3}$; and high concentrations of I/SVSOA were observed in central and northern
531 YRD. Overall, the addition of high-resolution I/SVOC emissions significantly increase
532 the SOA concentration by 148%, which will be further constrained by the observation
533 in next section.

534 To validate the model performance on regional OA simulation, we compared it
535 with the measured concentrations of organic carbon (OC) in $\text{PM}_{2.5}$ at multiple sites in
536 the YRD region (Figure S3). Although both BASE and I/SVOC-EIMPROVE
537 simulations showed good correlations with the observation as shown in Figures S3c,
538 S3f, S3i, and S3l, OC concentrations in I/SVOC-EIMPROVE simulations in different
539 seasons were all higher than those in the BASE simulations. In the BASE simulation,

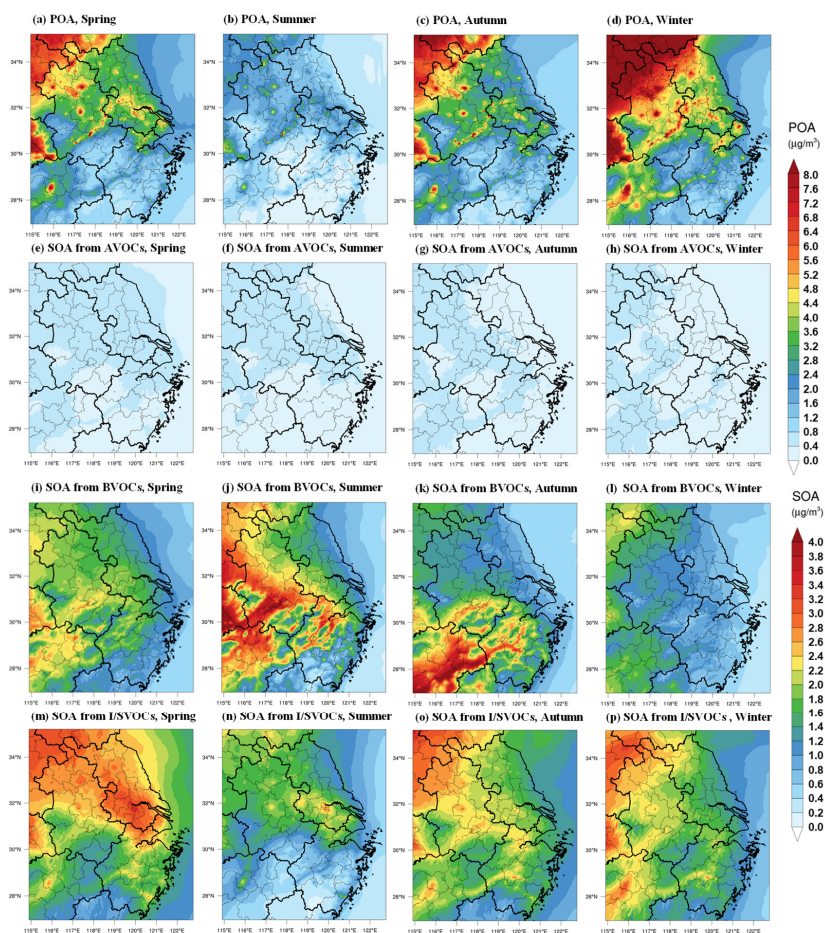
540 the modeled OC concentrations of each season only explained 51% to 71% of the
 541 observations. With the addition of I/SVOC emissions into I/SVOC-EIMPROVE
 542 simulation, the modeled OC concentrations much better agreed with the observations,
 543 with modeled OC increased to 70% to 91% of the observations. Details for the statistical
 544 evaluation of model performance on OC in BASE and I/SVOC-EIMPROVE
 545 simulations are shown in Table S7.

546



547

548 **Figure 5.** Comparisons of the regional average concentrations of POA and SOA formed from
 549 AVOCs, BVOCs, and I/SVOCs in different seasons from the BASE and I/SVOC-EIMPROVE
 550 simulations.



551
 552 **Figure 6.** Spatial distributions of modeled POA and SOA formed from AVOCs, BVOCs, and
 553 I/SVOCs in different seasons in the I/SVOC-EMPROVE simulation.

554 3.2.2 Temporal variations of OA components: simulation vs. AMS observation

555 To further validate the model performance on the simulations of POA and SOA,
 556 we compared the simulation results with those measured by an AMS at the SAES
 557 supersite. Both simulation and observation results were obtained for PM₁ aerosol
 558 particles (aerodynamic diameter < 1 μm). Note that uncertainty exist when directly
 559 compare the modeled OA factors with those resolved by AMS-PMF analysis since a
 560 clear split of POA and SOA from a measurement point of view can hardly be achieved.

561 To minimize the uncertainty associated with the PMF analysis, comprehensive
562 molecular identification of OA components was conducted and multiple source
563 apportionment model results were compared following the method in Huang et al.
564 (2021a) to improve the accuracy of the factor separation. Figure 7 shows that the
565 simulation results of POA, SOA and OA were similar to the observation results not only
566 in average concentration levels but also in temporal variations. For POA, the diurnal
567 patterns in the BASE and I/SVOC-EIMPROVE simulations agree with each other and
568 both can reproduce the observed concentrations. The POA concentrations in the
569 I/SVOC-EIMPROVE simulation cases decreased by 4%–18% (Figure S4) compared
570 with the BASE case and was closer to the observations. Similar to the observation
571 results, the simulated POA concentrations peaked at noon and early evening, which
572 were mainly contributed by cooking emissions as reported in our previous study (Huang
573 et al., 2021a).

574 For SOA, the average concentrations in spring, summer, autumn, and winter in
575 BASE simulation were 1.2, 1.6, 0.8, and 0.7 $\mu\text{g}\cdot\text{m}^{-3}$, respectively, which were only
576 14%–30% of those observed by the AMS (see Figure S4). The SOA simulation was
577 ~~greatly~~ improved in I/SVOC-EIMPROVE simulation with the modeled SOA
578 concentrations of 3.8 3.7, 2.7, and 2.3 $\mu\text{g}\cdot\text{m}^{-3}$ in spring, summer, autumn, and winter
579 respectively. The SOA concentrations in I/SVOC-EIMPROVE simulation were 2.4–3.6
580 times higher than those in BASE simulation, which ~~is~~ was 40% to 72% of the
581 observation, indicating the large contributions of I/SVOCs emissions to SOA
582 production.

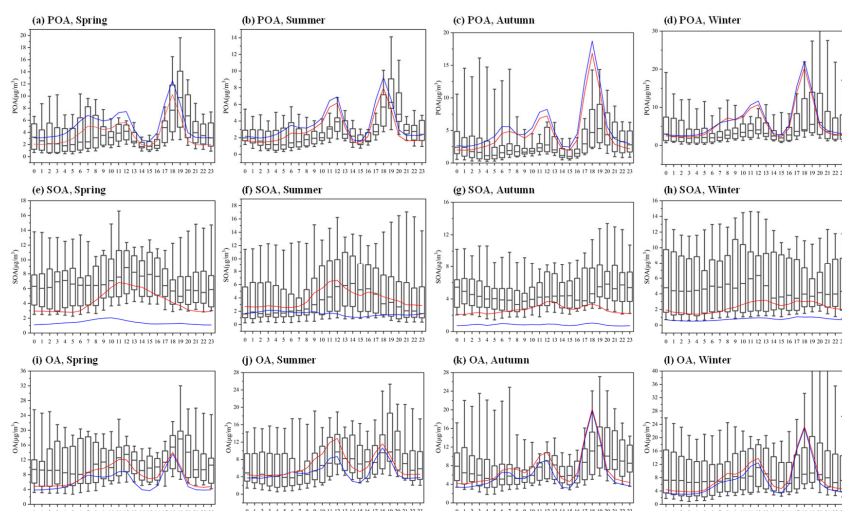
583 The I/SVOC-EIMPROVE simulation also demonstrated improvements in
584 reproducing the temporal variations of SOA, especially during the daytime (Figure
585 7e–7h). Compared with the BASE simulation, evident increases in SOA concentrations
586 during daytime can be observed in I/SVOC-EIMPROVE simulation (Figure 7e–7h),
587 which agrees better with the observation, likely driven by photochemistry. However,
588 the model is still hard to capture the diurnal patterns of SOA observed in most seasons.

589 ~~except for the summer. Although the SOA simulations were improved in all four~~
590 ~~seasons, best simulation results were found in summer,~~ when both the concentrations
591 and diurnal variations of SOA ~~were~~ are well reproduced, ~~which indicates that SOA in~~
592 ~~summer is mainly subject to photochemical oxidation of I/SVOC emissions, while SOA~~
593 ~~formation will be largely affected by other factors in other seasons, especially during~~
594 ~~the nighttime in cool seasons. For example,~~

595 ~~While our current results presented great improvements in SOA simulation, gaps~~
596 ~~were still left between the simulation and observation especially during the nighttime.~~
597 ~~The main reasons for the discrepancy between the simulated and measured SOA are:~~
598 ~~(1) I/SVOC emissions from outside of the YRD region might be underestimated due to~~
599 ~~the lack of detailed base emission inventory, resulting in the corresponding~~
600 ~~underestimation of the transported SOA, which were prominent especially in autumn,~~
601 ~~winter and spring in Shanghai; (2) current model simulation only consider the oxidation~~
602 ~~processes driven by OH oxidation. However, an increasing body of experimental and~~
603 observational evidence suggest that heterogeneous and multiphase reactions also played
604 important roles in SOA formation especially during pollution episodes (Guo et al., 2020;
605 Kim et al., ~~2021~~2022). Recent studies also found that nocturnal NO₃ oxidation was also
606 an important route for SOA formation, ~~which would drive the enhancement of SOA~~
607 ~~during the nighttime~~ (Yu et al., 2019; Decker et al., 2021). Yet mechanism and
608 parameterizations of these processes remain unclear, making the involvement of these
609 processes in the model difficult. ~~A recent study furtherly found that there were~~
610 ~~considerable emissions of condensable organic aerosols from stationary sources in the~~
611 ~~industrial and energy sectors, which would effectively improve the contributions of the~~
612 ~~industrial sector to OA simulation especially in winter, should also be considered in the~~
613 ~~future (Morino, et al., 2018; Morino, et al., 2022). In addition, I/SVOC emissions from~~
614 ~~outside of the YRD region might be underestimated due to the lack of detailed base~~
615 ~~emission inventory, resulting in the corresponding underestimation of the transported~~
616 ~~SOA, which were prominent especially in autumn, winter and spring in Shanghai. High-~~

617 resolution I/SVOCs emissions inventory is urgently needed to be developed at a larger
618 regional scale.

619
620 While our current results presented great improvements in SOA simulation, gaps
621 were still left between the simulation and observation especially during the nighttime.
622 The main reasons for the discrepancy between the simulated and measured SOA are:
623 (1) I/SVOC emissions from outside of the YRD region might be underestimated due to
624 the lack of detailed base emission inventory, resulting in the corresponding
625 underestimation of the transported SOA, which were prominent especially in autumn,
626 winter and spring in Shanghai; (2) current model simulation only consider the oxidation
627 processes driven by OH oxidation. However,



628
629 **Figure 7.** Diurnal patterns of modeled POA, SOA, and OA concentrations in different seasons and
630 their comparisons with the observations at the SAES supersite. The boxplots represent the diurnal
631 patterns of the AMS observations. The blue and red lines respectively represent the diurnal patterns
632 of the simulation results in BASE and I/SVOC-EMPROVE cases.

633 3.3 OA source contributions

634 3.3.1 POA and SOA sources in the region

635 Based on the high-resolution I/SVOC emission inventory established in this study,

636 we successfully simulated the POA and SOA concentrations from each source. Table 3
637 summarizes the regional average concentrations of POA and SOA originated from
638 different sources and their relative contributions. Residential POA dominated the
639 regional OA, with average concentrations ranged from 1.56 to 2.35-4 $\mu\text{g}\cdot\text{m}^{-3}$ in
640 different seasons, accounting for 19.475%-25.31% of the total OA, among which
641 cooking emission is the dominant source (*ca.* 98%) of residential POA. Other POA
642 sources include industrial, biomass burning, and mobile sources, accounting for
643 8.02%-8.63%, 4.45%-8.283%, and 5.03%-5.78% of the total OA, respectively. The
644 cumulative fraction of POA in total OA from industrial and mobile sources was
645 13.44%-14.41%, close to that of HOA (15%) observed by the AMS measurement in
646 Shanghai (Figure S5).

647 Industrial sources were the main source of SOA in the YRD region, with average
648 SOA concentrations of 0.84-1.2+ $\mu\text{g}\cdot\text{m}^{-3}$ in four seasons, accounting for
649 8.989.0%-15.64% of the total OA, among which, industrial process and solvent-use
650 sources had almost equal contributions. Mobile sources were the second largest source
651 of SOA in this region, with an average concentration of 0.34-0.50 $\mu\text{g}\cdot\text{m}^{-3}$, accounting
652 for 3.364%-6.697% of the total OA. Among them, the source contribution of gasoline
653 vehicles to SOA was 1.778%-3.071%, and that of diesel vehicles was 1.182%-2.556%.
654 BVSOA showed significant seasonal differences with concentrations of 0.889, 1.263,
655 0.70, and 0.1+ $\mu\text{g}\cdot\text{m}^{-3}$, respectively in spring, summer, autumn, and winter, accounting
656 for 9.64%, 16.94%, 7.60%, and 1.152% of the total OA.

657 Overall, cooking emission was the major source of POA in YRD, accounting for
658 19.14%-25.04.99% of the total OA, which is consistent with our observations in
659 Shanghai (Huang et al., 2021a; Zhu et al., 2021). Both simulations and observations
660 demonstrated higher contributions of cooking emission in urban China than those
661 reported overseas (17%-18%) (Chen et al., 2021), which is attributed to the difference
662 between Asian-style and Western-style cooking. The results emphasize that cooking
663 emission has become a non-negligible source of non-fossil carbon in urban areas in

664 eastern China. Contributions from industrial sources were running the second among
665 all sources, accounting for 17.02%–24.12% of OA and 24.7%–26.8% of SOA, which
666 is attributed to the high I/SVOC emissions from industrial sources and is consistent
667 with previous studies (Miao et al., 2021). Other sources mainly include mobile sources
668 (8.768% to 11.72% of OA) and biomass burning (5.192%–8.879% of OA). Specifically,
669 diesel and gasoline vehicles were the major contributors among mobile sources, with
670 higher contribution from the former (3.954.0%–4.667%) than the latter
671 (3.051%–4.02%), followed by diesel machinery (1.329%–2.14%) and marine vessels
672 (0.43%–0.93%). The contribution of biomass burning was highest in winter (8.879%)
673 compared to contributions of 5.192%–7.283% in other seasons and it was even higher
674 than contribution of mobile sources (8.76%) in winter. The remaining 14.54%–35.64%
675 of OA was from super region scale, which represented OA originated from emissions
676 outside the YRD region. Our results were generally similar with those of Chang et al.
677 (2022) for the YRD region. We both found the domestic combustion mainly engaged in
678 cooking emissions had a major contribution to OA. Next was volatile chemical products
679 (VCPs), especially the use of solvents, paints, and adhesives in industrial sector, also
680 made a high contribution. Note that industrial process also took up a high fraction in
681 our OA simulation, while it was lower in Chang et al. (2022)'s study. The difference in
682 I/SVOC emission estimates was the main reason for this divergence. Mobile sources in
683 both studies had similar contributions, which accounted for about 10% to total OA.
684 Comparatively, our source classification was more specific, which will help identify
685 more specific OA sources to design more refined regional control countermeasures.

686 **Table 3.** POA and SOA source contributions of different emission sources in each season in the
687 YRD region.

Sources	Spring		Summer		Autumn		Winter	
	conc.	ratio	conc.	ratio	conc.	ratio	conc.	ratio
	($\mu\text{g}\cdot\text{m}^{-3}$)	(%)	($\mu\text{g}\cdot\text{m}^{-3}$)	(%)	($\mu\text{g}\cdot\text{m}^{-3}$)	(%)	($\mu\text{g}\cdot\text{m}^{-3}$)	(%)
POA	4.47-5	49.19-2	3.09-1	41.65-7	5.05-1	55.06-1	6.09	64.29-3
Industrial sources	0.73	8.02	0.63	8.48-5	0.79-8	8.63	0.75-8	8.04
Industrial process	0.64	6.74	0.54	7.27-3	0.67	7.29-3	0.63	6.77-8

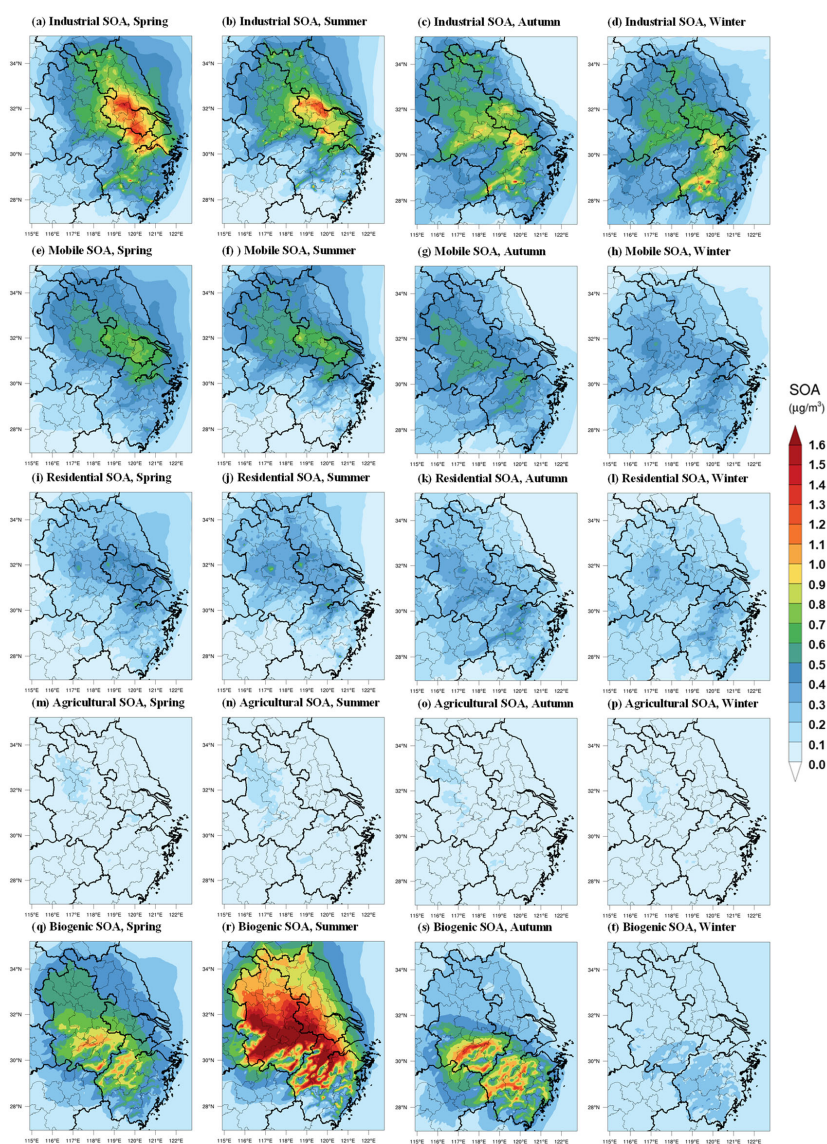
Industrial solvent-use	0.12	1.34	0.09-1	1.20	0.12	1.34	0.12	1.27-3
Mobile sources	0.49-5	5.43	0.37-4	5.03	0.53	5.78-8	0.50	5.40
Gasoline Vehicles	0.09-1	1.04	0.07-1	0.96-1.0	0.12	1.32	0.12	1.28
Diesel Vehicles	0.23	2.58-6	0.16-2	2.16-2	0.26-3	2.79-8	0.26-3	2.77-8
Diesel machinery	0.10	1.06-1	0.09-1	1.24	0.10	1.08-1	0.09-1	0.95-1.0
Marine vessel	0.07-1	0.78	0.05-1	0.70	0.05-1	0.59-6	0.04	0.39-4
Residential sources	1.77-8	19.47-5	1.56	20.95-1.0	2.32	25.34	2.35-4	25.16-2
Cooking	1.74	19.14	1.54	20.72	2.29-3	25.04-99	2.34	24.77-8
Other residential	0.03	0.33	0.02	0.23	0.03	0.33	0.04	0.39-4
Biomass burning	0.60	6.65-7	0.33	4.54-5	0.60	6.58-6	0.77-8	8.28-3
Super region	0.87-9	9.63	0.20	2.75-8	0.80	8.75-8	1.62	17.44
SOA	4.64	50.84	4.34	58.35-4	4.13	44.94	3.33	35.74
Industrial sources	1.24	13.38-4	1.16-2	15.64	1.02	11.10	0.84	89.0-98
Industrial process	0.68-7	7.53	0.62	8.39-4	0.64	6.62	0.53	5.64
Industrial solvent-use	0.53	5.84	0.54	7.25-3	0.44	4.48-5	0.34	3.34
Mobile sources	0.49-5	5.45-5	0.50	6.69-7	0.43	4.63	0.34	3.36-4
Gasoline Vehicles	0.25-3	2.74	0.23	3.07-1	0.24	2.25-3	0.16-2	1.77-8
Diesel Vehicles	0.18-2	2.04-95	0.19-2	2.50	0.16-2	1.73	0.14	1.18-2
Diesel machinery	0.06-1	0.66-7	0.07-1	0.90	0.05-1	0.56-6	0.03	0.37-4
Marine vessel	0.01	0.13	0.02	0.22	0.01	0.09-10	0.00	0.04
Residential sources	0.42	4.68-7	0.49-5	6.54	0.43	4.74	0.32	3.43-9
Cooking	0.24	2.34-3	0.29-3	3.974.0	0.26-3	2.78-8	0.16-2	1.74
Other residential	0.24	2.34	0.19-2	2.58-6	0.18-2	1.93	0.16-2	1.68-7
Biomass burning	0.06-1	0.63	0.06-1	0.74	0.05-1	0.65-9	0.06-1	0.60
Biogenic	0.88-9	9.64	1.26-3	16.94	0.70	7.60	0.14	1.45-2
Super region	1.55-6	17.04	0.88-9	11.80	1.50	16.30	1.70	18.23-2

688 3.3.2 Spatial distributions of SOA originated from different sources

689 Figure 8 shows the spatial distributions of modeled SOA originated from different
690 sources in each season in YRD region. Note that we only considered the SOA formed
691 from the intraregional VOC and I/SVOC emissions, excluding those transported from
692 the super region. A large spatial variability was observed for the sources of SOA driven
693 by emissions. For example, industrial and mobile SOA concentrated in the eastern and
694 central YRD, where I/SVOC emissions were high (Figure 4). Residential and
695 agricultural SOA presented a more uniform spatial distribution than industrial and
696 mobile SOA, with enhanced formation in central and western YRD (Figures 8i-8l).

697 Although absolute source-dependent SOA concentrations differ in different

698 seasons, low spatial variabilities were observed for different seasons. Industrial, mobile,
 699 and residential sources were the predominant contributors to SOA formation in eastern
 700 and central YRD, especially for the area along the Hangzhou Bay and Yangtze River
 701 driven by the enhanced I/SVOC emissions. The spatial distributions of BVSOA have
 702 been discussed above and will not be detailed here.



703

704 **Figure 8.** Spatial distributions of modeled SOA concentrations from different sources in each season
705 in YRD region.

706 3.3.3 Predominant OA sources in sub-regions of YRD

707 To characterize the source contributions in different parts of the region, we
708 categorized the simulation region into six sub-regions: northern YRD, western YRD,
709 central YRD, eastern YRD and southern YRD. And six representative cities in these
710 six regions were further selected for detailed comparison in source contributions,
711 including Xuzhou (XZ), Hefei (HF), Nanjing (NJ), Hangzhou (HZ), Shanghai (SH) and
712 Jinhua (JH). Figure 9 shows their locations and OA source contributions during summer
713 and winter.

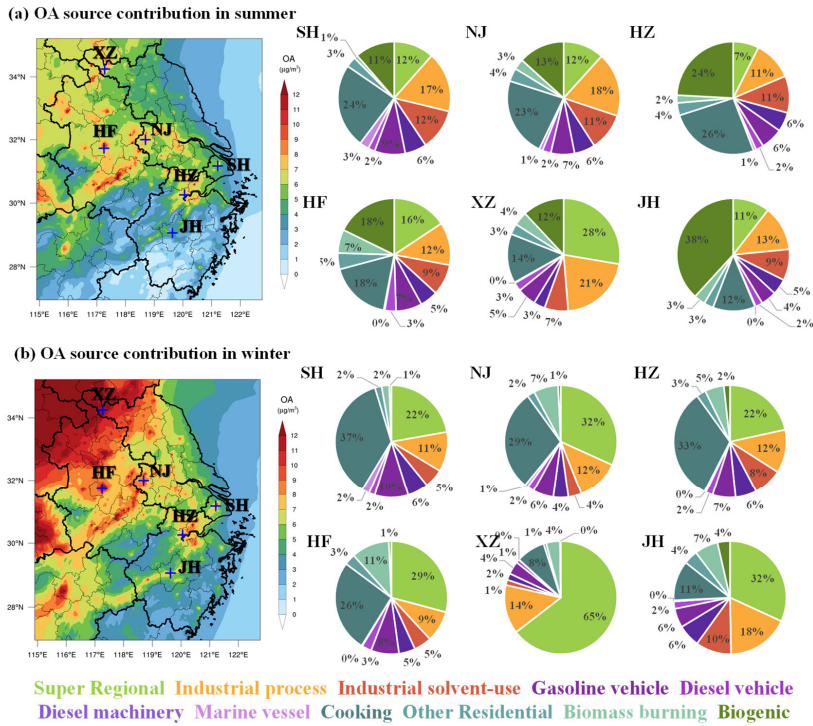
714 In Northern YRD, represented by XZ, enhanced contribution from super-regional
715 scale to the local OA was observed for both winter (64.6%) and summer (27.7%) and
716 the contributions from industrial processes (14.0% in winter and 21.0% in summer)
717 were also higher than other sub-regions. Other major sources include biogenic (12.0%)
718 and cooking emissions (14.1%) in summer and cooking (8.3%) in winter. Taken
719 together, super-regional transportation and industrial processes are predominant
720 contributors of OA in northern YRD, accounting for 78.6% and 48.7% in summer and
721 winter respectively, followed by cooking emissions.

722 In western YRD, represented by HF, cooking emission was the largest contributor
723 to OA with contributions of 17.8% and 26.3% in both summer and winter respectively,
724 followed by super-regional contributions of 15.7% (summer) and 29.2% (winter). Other
725 major sources also include mobile source of 15.5%, biogenic source in summer (17.8%)
726 and industrial processes in both summer (12.3%) and winter (8.9%). In central YRD,
727 represented by NJ and HZ, the relative source contributions were very similar to those
728 in western YRD, with predominant contributions from cooking (22.8%-32.6%),
729 followed by super-regional transportation (7.4%-31.8%), industrial processes (11.3%-
730 18.4%) and mobile source (13.1%-16.3%).

731 In eastern YRD, represented by SH, the largest OA source was cooking emission,
732 account for 24.3% and 36.6% of OA in summer and winter respectively, followed by

733 mobile sources of 19%, super-regional transportation of 11.5% (summer) and 22.2%
734 (winter) and industrial processes of 17.3% (summer) and 11.4% (winter). In southern
735 YRD, represented by JH, while biogenic contribution was prevailing in summer
736 (38.2%), super-regional transportation was significant in winter (31.8%). Similar to
737 other sub-regions, other major sources also included the contributions of cooking
738 emission of 12.2% (summer) and 11.4% (winter), industrial processes of 12.9%
739 (summer) and 17.9% (winter) and mobile sources of 13%. Yet southern YRD presented
740 more evident increase in the contribution from industrial solvent-use compared with
741 other sub-regions.

742 To summarize, cooking, super-regional transportation, industrial process and mobile
743 sources were the predominant sources of OA in all sub-regions regardless of the season,
744 albeit enhanced contributions from biogenic sources to the OA formation in summer
745 was observed, especially in southern YRD. High contributions of cooking sources were
746 in accordance with the distributions of populations and high contributions of mobile
747 sources were somewhat expected, especially in the city centers. Source contributions of
748 OA varies in the intraregional scale implies that more targeted control measures need
749 to be designed according to the emission features of each city. Specifically, for densely
750 populated area, it is necessary to strengthen the future control strategy of cooking
751 emissions; special attention needs to be paid to the I/SVOC emissions from industrial
752 sources in eastern, central, and northern YRD region; mobile sources show its
753 significance in urban area of the region, dominated by the equal contributions from
754 gasoline and diesel vehicles, indicating further reductions on the I/SVOCs from vehicle
755 emissions are therefore critical for pollution control on city scale.



756
 757 **Figure 9.** Source contributions of modeled OA concentrations from different sources during summer
 758 and winter in different cities of the region.

759 **4. Conclusions**

760 In this study, we established a high-resolution I/SVOC emission inventory with
 761 detailed source profiles and applied it into CMAQ v5.3 to simulate POA and SOA
 762 formation in YRD region of China. With the addition of I/SVOC emissions, simulation
 763 results show significant improvements on both temporal variations and spatial
 764 distributions of OA. Compared with the BASE simulation, where I/SVOC emissions
 765 were not included, the simulated SOA increased by 1.5 times in I/SVOC-EMPROVE
 766 simulation, highlighting the significant contributions of I/SVOC emissions to SOA
 767 production. The remaining 10%–30% underestimation of OA indicates that future work
 768 is still needed in bridging the gap between simulation and observations, such as,
 769 measuring local emission factors and source profiles of I/SVOC from various local

770 sources, updating SOA formation mechanisms in model framework.—

771 With the addition of source specific I/SVOC emissions, we successfully quantified
772 the contribution of each source to POA and SOA concentrations in YRD. For POA,
773 cooking emission is the predominant source, which concentrates in urban area of YRD
774 in accordance with the population distribution. For SOA, for the first time, we
775 demonstrate that I/SVOCs from industrial sources are dominant contributor, followed
776 by those from mobile sources. In summer, the contributions of biogenic emission to
777 total SOA are also non-negligible, especially for the cities in southern YRD. Spatial and
778 seasonal variations in the source contributions suggest that control strategies for OA
779 pollution should vary by cities and seasons. ~~For urban area~~On regional scale, cooking
780 emissions has been emerging as an important POA source, not to mention their impacts
781 on SOA formation are not yet certain. Our results suggest the control measures on the
782 cooking emissions should be strengthened in the future for the further reduction of POA.
783 ~~We also found that SOA in the region is primarily contributed by industrial I/SVOC~~
784 ~~emissions, which urges in-depth studies of emission factors and source profiles of~~
785 ~~I/SVOC emissions from industrial sources as well as the corresponding control~~
786 ~~measures. On intraregional scale, Another important source of SOA in urban area is~~
787 ~~mobile source, especially gasoline and diesel vehicles. Rfor urban area, continuous~~
788 ~~reduction in I/SVOC emissions from mobile sources, especially gasoline and diesel~~
789 ~~vehicles, are effective measures in the mitigation of urban air pollution, which is also~~
790 technically feasible as has been demonstrated in Qi et al. (2021). Continuous
791 improvement in emission standards is one way to promote the reduction of motor
792 vehicle related SOA. Our study further reveals that non-tailpipe sources of I/SVOCs
793 (e.g., solvent use, petrochemical, etc.) are major contributors to SOA formation in the
794 YRD region, consistent with Chang et al. (2022)'s model results in the national scale.
795 However, current understanding of SOA formation potentials from these sources are
796 still far from enough. For example, the localized I/SVOC emission factors and source
797 profiles of these sources are still missing. Their chemical behavior and SOA yields may

798 be different from the emissions from mobile sources which have been widely studied,
799 which urges in-depth studies on these sources as well as the corresponding control
800 measures.

801 *Data availability*

802 The gridded emissions of I/SVOCs from various sources for the YRD region
803 developed by this study at a horizontal resolution of 4 km × 4 km can be downloaded
804 from the following website (<https://doi.org/10.6084/m9.figshare.19536082.v1>).
805 Additional related data are available upon request by contacting the corresponding
806 author (Cheng Huang; huangc@saes.sh.cn).

807 *Supplement*

808 The supplement related to this article is available online.

809 *Author contributions*

810 CH, JA, DH, and MQ designed the research. CH and JA developed the I/SVOC
811 emission inventory. JA, MQ, and RY performed the model. DH, LQ, MZ, YL, SZ, and
812 QW collected the observation data. CH, JA, DH, and HW analyzed the results. CH, JA,
813 and DH wrote the paper.

814 *Competing interests*

815 The authors declare that they have no conflict of interest.

816 *Acknowledgement*

817 We thank the supports from the National Natural Science Foundation of China, the
818 Science and Technology Commission of the Shanghai Municipality, and the Shanghai
819 Municipal Bureau of Ecology and Environment.

820 *Financial support*

821 This work has been supported by the National Natural Science Foundation of
822 China (grant nos. 21777101), the Science and Technology Commission of the Shanghai
823 Municipality (grant no. 21230711000), the Shanghai Municipal Bureau of Ecology and

824 Environment Fund Project (grant no. 202001; 202114), and the State Environmental
825 Protection Key Laboratory of Formation and Prevention of Urban Air Pollution
826 Complex (grant no. CX2020080576).

827 **References**

- 828 An, J., Huang, Y., Huang, C., Wang, X., Yan, R., Wang, Q., Wang, H., Jing, S., Zhang, Y., Liu,
829 Y., Chen, Y., Xu, C., Qiao, L., Zhou, M., Zhu, S., Hu, Q., Lu, J., and Chen, C.: Emission
830 inventory of air pollutants and chemical speciation for specific anthropogenic sources
831 based on local measurements in the Yangtze River Delta region, China, *Atmos. Chem.*
832 *Phys.*, 21, 2003–2025, 2021.
- 833 Boylan, J. W., and Russell, A. G.: PM and light extinction model performance metrics, goals,
834 and criteria for three-dimensional air quality models, *Atmos. Environ.*, 40, 4946–4959,
835 2006.
- 836 Cai, S., Zhu, L., Wang, S., Wisthaler, A., Li, Q., Jiang, J., and Hao, J.: Time-resolved
837 intermediate-volatility and semivolatile organic compound emissions from household coal
838 combustion in northern China, *Environ. Sci. Technol.*, 53, 9269–9278, 2019.
- 839 Canagaratna, M. R., Jayne, J. T., Jimenez, J. L., Allan, J. D., Alfarra, M. R., Zhang, Q., Onasch,
840 T. B., Drewnick, F., Coe, H., Middlebrook, A., Delia, A., Williams, L. R., Trimborn, A. M.,
841 Northway, M. J., DeCarlo, P. F., Kolb, C. E., Davidovits, P., and Worsnop, D. R.: Chemical
842 and microphysical characterization of ambient aerosols with the aerodyne aerosol mass
843 spectrometer, *Mass Spectrom. Rev.*, 26, 185–222, 2007.
- 844 Canonaco, F., Crippa, M., Slowik, J. G., Baltensperger, U., and Prévôt, A. S. H.: SoFi, an IGOR-
845 based interface for the efficient use of the generalized multilinear engine (ME-2) for the
846 source apportionment: ME-2 application to aerosol mass spectrometer data, *Atmos. Meas.*
847 *Tech.*, 6, 3649–3661, 2013.
- 848 Chang, X., Zhao, B., Zheng, H., Wang, S., Cai, S., Guo, F., Gui, P., Huang, G., Wu, D., Han, L.,
849 Xing, J., Man, H., Hu, R., Liang, C., Xu, Q., Qiu, X., Ding, D., Liu, K., Han, R., Robinson,
850 A. L., and Donahue, N. M.: Full-volatility emission framework corrects missing and
851 underestimated secondary organic aerosol sources, *One Earth*, 5, 403–412, 2022.

852 Chen, W., Ye, Y., Hu, W., Zhou, H., Pan, T., Wang, Y., Song, W., Song, Q., Ye, C., Wang, C.,
853 Wang, B., Huang, S., Yuan, B., Zhu, M., Lian, X., Zhang, G., Bi, X., Jiang, F., Liu, J.,
854 Canonaco, F., Prevot, A. S. H., Shao, M., and Wang, X.: Real-time characterization of
855 aerosol compositions, sources, and aging processes in Guangzhou during PRIDE-GBA
856 2018 campaign, *J. Geophys. Res., Atmos.*, 126, e2021JD035114, 2021.

857 Crippa, M., Canonaco, F., Lanz, V. A., Äijälä, M., Allan, J. D., Carbone, S., Capes, G., Ceburnis,
858 D., Dall'Osto, M., Day, D. A., DeCarlo, P. F., Ehn, M., Eriksson, A., Freney, E.,
859 Hildebrandt Ruiz, L., Hillamo, R., Jimenez, J. L., Junninen, H., Kiendler-Scharr, A.,
860 Kortelainen, A. M., Kulmala, M., Laaksonen, A., Mensah, A. A., Mohr, C., Nemitz, E.,
861 O'Dowd, C., Ovadnevaite, J., Pandis, S. N., Petäjä, T., Poulain, L., Saarikoski, S., Sellegri,
862 K., Swietlicki, E., Tiitta, P., Worsnop, D. R., Baltensperger, U., and Prévôt, A. S. H.:
863 Organic aerosol components derived from 25 AMS data sets across Europe using a
864 consistent ME-2 based source apportionment approach, *Atmos. Chem. Phys.*, 14, 6159–
865 6176, 2014.

866 Cross, E. S., Hunter, J. F., Carrasquillo, A. J., Franklin, J. P., Herndon, S. C., Jayne, J. T.,
867 Worsnop, D. R., Miake-Lye, R. C., and Kroll, J. H.: Online measurements of the emissions
868 of intermediate-volatility and semi-volatile organic compounds from aircraft, *Atmos.*
869 *Chem. Phys.*, 13, 7845–7858, 2013.

870 Decker, Z. C. J., Robinson, M. A., Barsanti, K. C., Bourgeois, I., Coggon, M. M., DiGangi, J.
871 P., Diskin, G. S., Flocke, F. M., Franchin, A., Fredrickson, C. D., Gkatzelis, G. I., Hall, S.
872 R., Halliday, H., Holmes, C. D., Gregory Huey, L., Lee, Y. R., Lindaas, J., Middlebrook,
873 A. M., Montzka, D. D., Moore, R., Andrew Neuman, J., Nowak, J. B., Palm, B. B., Peischl,
874 J., Piel, F., Rickly, P. S., Rollins, A. W., Ryerson, T. B., Schwantes, R. H., Sekimoto, K.,
875 Thornhill, L., Thornton, J. A., Tyndall, G. S., Ullmann, K., Van Rooy, P., Veres, P. R.,
876 Warneke, C., Washenfelder, R. A., Weinheimer, A. J., Wiggins, E., Winstead, E., Wisthaler,
877 A., Womack, C., and Brown, S. S.: Nighttime and daytime dark oxidation chemistry in
878 wildfire plumes: an observation and model analysis of FIREX-AQ aircraft data, *Atmos.*
879 *Chem. Phys.*, 21, 16293–16317, 2021.

880 Donahue, N. M., Robinson, A. L., and Pandis, S. N.: Atmospheric organic particulate matter:
881 From smoke to secondary organic aerosol, *Atmos. Environ.*, 43, 94–106, 2009.

882 Donahue, N. M., Robinson, A. L., Stanier, C. O., and Pandis, S. N.: Coupled Partitioning,
883 Dilution, and Chemical Aging of Semivolatile Organics, *Environ. Sci. Technol.*, 40, 2635–
884 2643, 2006.

885 Drozd, G. T., Weber, R. J., and Goldstein, A. H.: Highly resolved composition during diesel
886 evaporation with modeled ozone and secondary aerosol formation: Insights into pollutant
887 formation from evaporative intermediate volatility organic compound sources, *Environ.*
888 *Sci. Technol.*, 55, 5742–5751, 2021.

889 Drozd, G. T., Zhao, Y., Saliba, G., Frodin, B., Maddox, C., Oliver Chang, M.-C., Maldonado,
890 H., Sardar, S., Weber, R. J., Robinson, A. L., and Goldstein, A. H.: Detailed speciation of
891 intermediate volatility and semivolatile organic compound emissions from gasoline
892 vehicles: Effects of cold-starts and implications for secondary organic aerosol formation,
893 *Environ. Sci. Technol.*, 53, 1706–1714, 2019.

894 Emery, C., Tai, E., and Yarwood, G.: Enhanced meteorological modeling and performance
895 evaluation for two Texas ozone episodes, Prepared for the Texas natural resource
896 conservation commission, by ENVIRON International Corporation, 2001.

897 Gentner, D. R., Isaacman, G., Worton, D. R., Chan, A. W. H., Dallmann, T. R., Davis, L., Liu,
898 S., Day, D. A., Russell, L. M., Wilson, K. R., Weber, R., Guha, A., Harley, R. A., and
899 Goldstein, A. H.: Elucidating secondary organic aerosol from diesel and gasoline vehicles
900 through detailed characterization of organic carbon emissions, *Proc. Natl. Acad. Sci.*, 109,
901 18318–18323, 2012.

902 Guo, J., Zhou, S., Cai, M., Zhao, J., Song, W., Zhao, W., Hu, W., Sun, Y., He, Y., Yang, C., Xu,
903 X., Zhang, Z., Cheng, P., Fan, Q., Hang, J., Fan, S., Wang, X., and Wang, X.:
904 Characterization of submicron particles by time-of-flight aerosol chemical speciation
905 monitor (ToF-ACSM) during wintertime: aerosol composition, sources, and chemical
906 processes in Guangzhou, China, *Atmos. Chem. Phys.*, 20, 7595–7615, 2020.

907 Hallquist, M., Wenger, J. C., Baltensperger, U., Rudich, Y., Simpson, D., Claeys, M., Dommen,

908 J., Donahue, N. M., George, C., Goldstein, A. H., Hamilton, J. F., Herrmann, H., Hoffmann,
909 T., Iinuma, Y., Jang, M., Jenkin, M. E., Jimenez, J. L., Kiendler-Scharr, A., Maenhaut, W.,
910 McFiggans, G., Mentel, Th. F., Monod, A., Prévôt, A. S. H., Seinfeld, J. H., Surratt, J. D.,
911 Szmigielski, R., and Wildt, J.: The formation, properties and impact of secondary organic
912 aerosol: Current and emerging issues, *Atmos. Chem. Phys.*, 9, 5155–5236, 2009.

913 Hayes, P. L., Ortega, A. M., Cubison, M. J., Froyd, K. D., Zhao, Y., Cliff, S. S., Hu, W. W.,
914 Toohey, D. W., Flynn, J. H., Lefer, B. L., Grossberg, N., Alvarez, S., Rappenglück, B.,
915 Taylor, J. W., Allan, J. D., Holloway, J. S., Gilman, J. B., Kuster, W. C., de Gouw, J. A.,
916 Massoli, P., Zhang, X., Liu, J., Weber, R. J., Corrigan, A. L., Russell, L. M., Isaacman, G.,
917 Worton, D. R., Kreisberg, N. M., Goldstein, A. H., Thalman, R., Waxman, E. M., Volkamer,
918 R., Lin, Y. H., Surratt, J. D., Kleindienst, T. E., Offenberg, J. H., Dusanter, S., Griffith, S.,
919 Stevens, P. S., Brioude, J., Angevine, W. M., and Jimenez, J. L.: Organic aerosol
920 composition and sources in Pasadena, California, during the 2010 CalNex campaign, *J.*
921 *Geophys. Res., Atmos.*, 118, 9233–9257, 2013.

922 Huang, C., Hu, Q., Li, Y., Tian, J., Ma, Y., Zhao, Y., Feng, J., An, J., Qiao, L., Wang, H., Jing,
923 S., Huang, D., Lou, S., Zhou, M., Zhu, S., Tao, S., and Li, L.: Intermediate volatility
924 organic compound emissions from a large cargo vessel operated under real-world
925 conditions, *Environ. Sci. Technol.*, 52, 12934–12942, 2018.

926 Huang, D., Zhu, S., An, J., Wang, Q., Qiao, L., Zhou, M., He, X., Ma, Y., Sun, Y., Huang, C.,
927 Yu, J., and Zhang, Q.: Comparative assessment of cooking emission contributions to urban
928 organic aerosol using online molecular tracers and aerosol mass spectrometry
929 measurements, *Environ. Sci. Technol.*, 55, 14526–14535, 2021a.

930 Huang, L., Wang, Q., Wang, Y., Emery, C., Zhu, A., Zhu, Y., Yin, S., Yarwood, G., Zhang, K.,
931 and Li, L.: Simulation of secondary organic aerosol over the Yangtze River Delta region:
932 The impacts from the emissions of intermediate volatility organic compounds and the SOA
933 modeling framework, *Atmos. Environ.*, 246, 118079, 2021b.

934 Huang, R. J., Zhang, Y., Bozzetti, C., Ho, K., Cao, J., Han, Y., Daellenbach, K. R., Slowik, J.
935 G., Platt, S. M., Canonaco, F., Zotter, P., Wolf, R., Pieber, S. M., Bruns, E. A., Crippa, M.,

936 Ciarelli, G., Piazzalunga, A., Schwikowski, M., Abbaszade, G., Schnelle-Kreis, J.,
937 Zimmermann, R., An, Z., Szidat, S., Baltensperger, U., El Haddad, I., and Prévôt, A. S. H.:
938 High secondary aerosol contribution to particulate pollution during haze events in China,
939 *Nature*, 514, 218–222, 2014.

940 Huffman, J., Docherty, K., Mohr, C., Cubison, M., Ulbrich, I., Ziemann, P., Onasch, T., and
941 Jimenez, J.: Chemically-resolved volatility measurements of organic aerosol from
942 different sources, *Environ. Sci. Technol.*, 43, 5351–5357, 2009.

943 Jathar, S. H., Gordon, T. D., Hennigan, C. J., Pye, H. O. T., Pouliot, G., Adams, P. J., Donahue,
944 N. M., and Robinson, A. L.: Unspeciated organic emissions from combustion sources and
945 their influence on the secondary organic aerosol budget in the United States, *P. Natl. Acad.*
946 *Sci. USA*, 111, 10473–10478, 2014.

947 Jathar, S. H., Woody, M., Pye, H. O. T., Baker, K. R., and Robinson, A. L.: Chemical transport
948 model simulations of organic aerosol in southern California: model evaluation and
949 gasoline and diesel source contributions, *Atmos. Chem. Phys.*, 17, 4305–4318, 2017.

950 Jimenez, J. L., Canagaratna, M. R., Donahue, N. M., Prevot, A. S. H., Zhang, Q., Kroll, J. H.,
951 DeCarlo, P. F., Allan, J. D., Coe, H., Ng, N. L., Aiken, A. C., Docherty, K. S., Ulbrich, I.
952 M., Grieshop, A. P., Robinson, A. L., Duplissy, J., Smith, J. D., Wilson, K. R., Lanz, V. A.,
953 Hueglin, C., Sun, Y. L., Tian, J., Laaksonen, A., Raatikainen, T., Rautiainen, J., Vaattovaara,
954 P., Ehn, M., Kulmala, M., Tomlinson, J. M., Collins, D. R., Cubison, M. J., Dunlea, J.,
955 Huffman, J. A., Onasch, T. B., Alfarra, M. R., Williams, P. I., Bower, K., Kondo, Y.,
956 Schneider, J., Drewnick, F., Borrmann, S., Weimer, S., Demerjian, K., Salcedo, D., Cottrell,
957 L., Griffin, R., Takami, A., Miyoshi, T., Hatakeyama, S., Shimono, A., Sun, J. Y., Zhang,
958 Y. M., Dzepina, K., Kimmel, J. R., Sueper, D., Jayne, J. T., Herndon, S. C., Trimborn, A.
959 M., Williams, L. R., Wood, E. C., Middlebrook, A. M., Kolb, C. E., Baltensperger, U., and
960 Worsnop, D. R.: Evolution of Organic Aerosols in the Atmosphere, *Science*, 326, 1525–
961 1529, 2009.

962 Kim, D., Cho, C., Jeong, S., Lee, S., Nault, B. A., Campuzano-Jost, P., Day, D. A., Schroder, J.
963 C., Jimenez, J. L., Volkamer, R., Blake, D. R., Wisthaler, A., Fried, A., DiGangi, J. P.,

964 Diskin, G. S., Pusede, S. E., Hall, S. R., Ullmann, K., Gregory Huey, L., Tanner, D. J.,
965 Dibb, J., Knote, C. J., and Min, K., Field observational constraints on the controllers in
966 glyoxal (CHOCHO) reactive uptake to aerosol, *Atmos. Chem. Phys.*, 22, 805–821, 2022.

967 Kim, Y., Couvidat, F., Sartelet, K., and Seigneur, C.: Comparison of different gas-phase
968 mechanisms and aerosol modules for simulating particulate matter formation, *J. Air Waste*
969 *Manage.*, 61, 1218–1226, 2011.

970 Koo, B., Knipping, E., and Yarwood, G.: 1.5-Dimensional volatility basis set approach for
971 modeling organic aerosol in CAMx and CMAQ, *Atmos. Environ.*, 95, 158–164, 2014.

972 Koss, A. R., Sekimoto, K., Gilman, J. B., Selimovic, V., Coggon, M. M., Zarzana, K. J., Yuan,
973 B., Lerner, B. M., Brown, S. S., Jimenez, J. L., Krechmer, J., Roberts, J. M., Warneke, C.,
974 Yokelson, R. J., and de Gouw, J.: Non-methane organic gas emissions from biomass
975 burning: identification, quantification, and emission factors from PTR-ToF during the
976 FIREX 2016 laboratory experiment, *Atmos. Chem. Phys.*, 18, 3299–3319, 2018.

977 Li, J., Cao, L., Gao, W., He, L., Yan, Y., He, Y., Pan, Y., Ji, D., Liu, Z., and Wang, Y.: Seasonal
978 variations in the highly time-resolved aerosol composition, sources and chemical
979 processes of background submicron particles in the North China Plain, *Atmos. Chem.*
980 *Phys.*, 21, 4521–4539, 2021.

981 Li, J., Han, Z., Li, J., Liu, R., Wu, Y., Liang, L., and Zhang, R.: The formation and evolution of
982 secondary organic aerosol during haze events in Beijing in wintertime, *Sci. Total Environ.*,
983 703, 134937, 2020.

984 Li, J., Han, Z., Wu, J., Tao, J., Li, J., Sun, Y., Liang, L., Liang, M., and Wang, Q.: Secondary
985 organic aerosol formation and source contributions over east China in summertime,
986 *Environ. Pollut.*, 306, 119383, 2022.

987 Li, M., Zhang, Q., Kurokawa, J. i., Woo, J. H., He, K., Lu, Z., Ohara, T., Song, Y., Streets, D.
988 G., Carmichael, G. R., Cheng, Y., Hong, C., Huo, H., Jiang, X., Kang, S., Liu, F., Su, H.,
989 Zheng, B.: MIX: a mosaic Asian anthropogenic emission inventory under the international
990 collaboration framework of the MICS-Asia and HTAP. *Atmos. Chem. Phys.*, 17, 935–963,
991 2017.

992 Li, Y., Ren, B., Qiao, Z., Zhu, J., Wang, H., Zhou, M., Qiao, L., Lou, S., Jing, S., Huang, C.,
993 Tao, S., Rao, P., and Li, J.: Characteristics of atmospheric intermediate volatility organic
994 compounds (IVOCs) in winter and summer under different air pollution levels, *Atmos.*
995 *Environ.*, 210, 58–65, 2019.

996 Li, Y. J., Sun, Y. L., Zhang, Q., Li, X., Li, M., Zhou, Z., and Chan, C. K.: Real-time chemical
997 characterization of atmospheric particulate matter in China: A review, *Atmos. Environ.*,
998 158, 270–304, 2017.

999 Liggio, J., Li, S., Hayden, K., Taha, Y. M., Stroud, C., Darlington, A., Drollette, B. D., Gordon,
1000 M., Lee, P., Liu, P., Leithead, A., Moussa, S. G., Wang, D., Brien, J. O., Mittermeier, R.
1001 L., Osthoff, H. D., Makar, P. A., Zhang, J., Brook, J. R., Lu, G., Staebler, R. M., Han, Y.,
1002 Travis, W., Plata, D. L., and Gentner, D. R.: Oil sands operations as a large source of
1003 secondary organic aerosols, *Nature*, 534, 1–16, 2016.

1004 Ling, Z., Wu, L., Wang, Y., Shao, M., Wang, X., and Huang, W.: Roles of semivolatile and
1005 intermediate-volatility organic compounds in secondary organic aerosol formation and its
1006 implication: A review, *J. Environ. Sci.*, 114, 259–285, 2022.

1007 Liu, H., Man, H., Cui, H., Wang, Y., Deng, F., Wang, Y., Yang, X., Xiao, Q., Zhang, Q., Ding,
1008 Y., and He, K.: An updated emission inventory of vehicular VOCs and IVOCs in China,
1009 *Atmos. Chem. Phys.*, 17, 12709–12724, 2017.

1010 Liu, H., Meng, Z., Lv, Z., Wang, X., Deng, F., Liu, Y., Zhang, Y., Shi, M., Zhang, Q., and He,
1011 K.: Emissions and health impacts from global shipping embodied in US–China bilateral
1012 trade, *Nat. Sustain.*, 2, 1027–1033, 2019.

1013 Liu, Y., Li, L., An, J., Huang, L., Yan, R., Huang, C., Wang, H., Wang, Q., Wang, M., and Zhang,
1014 W.: Estimation of biogenic VOC emissions and its impact on ozone formation over the
1015 Yangtze River Delta region, China, *Atmos. Environ.*, 186, 113–128, 2018a.

1016 Liu, Z., Gao, W., Yu, Y., Hu, B., Xin, J., Sun, Y., Wang, L., Wang, G., Bi, X., Zhang, G., Xu, H.,
1017 Cong, Z., He, J., Xu, J., and Wang, Y.: Characteristics of PM_{2.5} mass concentrations and
1018 chemical species in urban and background areas of China: emerging results from the
1019 CARE-China network, *Atmos. Chem. Phys.*, 18, 8849–8871, 2018b.

设置了格式: 下标

1020 Louvaris, E. E., Florou, K., Karnezi, E., Papanastasiou, D. K., Gkatzelis, G. I., and Pandis, S.
1021 N.: Volatility of source apportioned wintertime organic aerosol in the city of Athens,
1022 Atmos. Environ., 158, 138–147, 2017.

1023 Lu, Q., Murphy, B. N., Qin, M., Adams, P. J., Zhao, Y., Pye, H. O. T., Efstathiou, C., Allen, C.,
1024 and Robinson, A. L.: Simulation of organic aerosol formation during the CalNex study:
1025 Updated mobile emissions and secondary organic aerosol parameterization for
1026 intermediate-volatility organic compounds, Atmos. Chem. Phys., 20, 4313–4332, 2020.

1027 Lu, Q., Zhao, Y., and Robinson, A. L.: Comprehensive organic emission profiles for gasoline,
1028 diesel, and gas-turbine engines including intermediate and semi-volatile organic
1029 compound emissions, Atmos. Chem. Phys., 18, 17637–17654, 2018.

1030 May, A. A., Levin, E. J. T., Hennigan, C. J., Riipinen, I., Lee, T., Collett, J. L., Jimenez, J. L.,
1031 Kreidenweis, S. M., and Robinson, A. L.: Gas-particle partitioning of primary organic
1032 aerosol emissions: 3. Biomass burning, J. Geophys. Res.-Atmos., 118, 11327–11338, 2013.

1033 McDonald, B. C., de Gouw, J. A., Gilman, J. B., Jathar, S. H., Akherati, A., Cappa, C. D.,
1034 Jimenez, J. L., Lee-Taylor, J., Hayes, P. L., McKeen, S. A., Cui, Y. Y., Kim, S., Gentner,
1035 D. R., Isaacman-VanWertz, G., Goldstein, A. H., Harley, R. A., Frost, G. J., Roberts, J. M.,
1036 Ryerson, T. B., and Trainer, M.: Volatile chemical products emerging as largest
1037 petrochemical source of urban organic emissions, Science, 359, 760–764, 2018.

1038 Miao, R., Chen, Q., Shrivastava, M., Chen, Y., Zhang, L., Hu, J., Zheng, Y., and Liao, K.:
1039 Process-based and observation-constrained SOA simulations in China: the role of
1040 semivolatile and intermediate-volatility organic compounds and OH levels, Atmos. Chem.
1041 Phys., 21, 16183–16201, 2021.

1042 Ming, L., Jin, L., Li, J., Fu, P., Yang, W., Liu, D., Zhang, G., Wang, Z., and Li, X.: PM_{2.5} in the
1043 Yangtze River Delta, China: Chemical compositions, seasonal variations, and regional
1044 pollution events, Environ. Pollut., 223, 200–212, 2017.

1045 [Morino, Y., Chatani, S., Tanabe, K., Fujitani, Y., Morikawa, T., Takahashi, K., Sato, K., and](#)
1046 [Sugata, S.: Contributions of condensable particulate matter to atmospheric organic aerosol](#)
1047 [over Japan, Environ. Sci. Technol., 52, 8456–8466, 2018.](#)

1048 [Morino, Y., Chatani, S., Fujitani, Y., Tanabe, K., Murphy, B. N., Jathar, S. H., Takahashi, K.,](#)
1049 [Sato, K., Kumagai, K., and Saito, S.: Emissions of condensable organic aerosols from](#)
1050 [stationary combustion sources over Japan. *Atmos. Environ.*, 289, 119319, 2022.](#)

1051 Murphy, B. N., Woody, M. C., Jimenez, J. L., Carlton, A. M. G., Hayes, P. L., Liu, S., Ng, N.
1052 L., Russell, L. M., Setyan, A., and Xu, L.: Semivolatile POA and parameterized total
1053 combustion SOA in CMAQv5.2: impacts on source strength and partitioning, *Atmos.*
1054 *Chem. Phys.*, 17, 11107–11133, 2017.

1055 Nault, B. A., Jo, D. S., McDonald, B. C., Campuzano-Jost, P., Day, D. A., Hu, W., Schroder, J.
1056 C., Allan, J., Blake, D. R., Canagaratna, M. R., Coe, H., Coggon, M. M., DeCarlo, P. F.,
1057 Diskin, G. S., Dunmore, R., Flocke, F., Fried, A., Gilman, J. B., Gkatzelis, G., Hamilton,
1058 J. F., Hanisco, T. F., Hayes, P. L., Henze, D. K., Hodzic, A., Hopkins, J., Hu, M., Huey, L.
1059 G., Jobson, B. T., Kuster, W. C., Lewis, A., Li, M., Liao, J., Nawaz, M. O., Pollack, I. B.,
1060 Peischl, J., Rappenglück, B., Reeves, C. E., Richter, D., Roberts, J. M., Ryerson, T. B.,
1061 Shao, M., Sommers, J. M., Walega, J., Warneke, C., Weibring, P., Wolfe, G. M., Young, D.
1062 E., Yuan, B., Zhang, Q., de Gouw, J. A., and Jimenez, J. L.: Secondary organic aerosols
1063 from anthropogenic volatile organic compounds contribute substantially to air pollution
1064 mortality, *Atmos. Chem. Phys.*, 21, 11201–11224, 2021.

1065 Presto, A. A., Miracolo, M. A., Kroll, J. H., Worsnop, D. R., Robinson, A. L., and Donahue, N.
1066 M.: Intermediate-volatility organic compounds: A potential source of ambient oxidized
1067 organic aerosol, *Environ. Sci. Technol.*, 43, 4744–4749, 2009.

1068 Presto, A. A., Nguyen, N. T., Ranjan, M., Reeder, A. J., Lipsky, E. M., Hennigan, C. J., Miracolo,
1069 M. A., Riemer, D. D., and Robinson, A. L.: Fine particle and organic vapor emissions from
1070 staged tests of an in-use aircraft engine, *Atmos. Environ.*, 45, 3603–3612, 2011.

1071 Pye, H. O. T., Seinfeld, J. H.: A global perspective on aerosol from low-volatility organic
1072 compounds, *Atmos. Chem. Phys.*, 10, 4377–4401, 2010.

1073 Qi, L., Liu, H., Shen, X., Fu, M., Huang, F., Man, H., Deng, F., Shaikh, A. A., Wang, X., Dong,
1074 R., Song, C., and He, K.: Intermediate-volatility organic compound emissions from
1075 nonroad construction machinery under different operation modes, *Environ. Sci. Technol.*,

1076 53, 13832–13840, 2019.

1077 Qi, L., Zhao, J., Li, Q., Su, S., Lai, Y., Deng, F., Man, H., Wang, X., Shen, X., Lin, Y., Ding, Y.,
1078 and Liu, H.: Primary organic gas emissions from gasoline vehicles in China: Factors,
1079 composition and trends, *Environ. Pollut.*, 290, 117984, 2021.

1080 Qin, M., Hu, A., Mao, J., Li, X., Sheng, L., Sun, J., Li, J., Wang, X., Zhang, Y., Hu, J.: PM_{2.5}
1081 and O₃ relationships affected by the atmospheric oxidizing capacity in the Yangtze River
1082 Delta, China, *Sci. Total Environ.*, 810, 152268, 2022.

1083 Ren, B., Zhu, J., Tian, L., Wang, H., Huang, C., Jing, S., Lou, S., An, J., Lu, J., Rao, P., Fu, Q.,
1084 Huo, J., and Li, Y.: An alternative semi-quantitative GC/MS method to estimate levels of
1085 airborne intermediate volatile organic compounds (IVOCs) in ambient air, *Atmos.*
1086 *Environ.*, X6, 100075, 2020.

1087 Robinson, A. L., Donahue, N. M., Shrivastava, M. K., Weitkamp, E. A., Sage, A. M., Grieshop,
1088 A. P., Lane, T. E., Pierce, J. R., and Pandis, S. N.: Rethinking organic aerosols:
1089 Semivolatile emissions and photochemical aging, *Science*, 315, 1259–1262, 2007.

1090 Sartelet, K., Zhu, S., Moukhtar, S., André, M., Gros, V., Favez, O., Brasseur, A., and Redaelli,
1091 M.: Emission of intermediate, semi and low volatile organic compounds from traffic and
1092 their impact on secondary organic aerosol concentrations over greater paris, *Atmos.*
1093 *Environ.*, 180, 126–137, 2018.

1094 Shrivastava, M. K., Cappa, C. D., Fan, J., Goldstein, A. H., Guenther, A. B., Jimenez, J. L.,
1095 Kuang, C., Laskin, A., Martin, S. T., Ng, N. L., Petaja, T., Pierce, J. R., Rasch, P. J., Roldin,
1096 P., Seinfeld, J. H., Shilling, J., Smith, J. N., Thornton, J. A., Volkamer, R., Wang, J.,
1097 Worsnop, D. R., Zaveri, R. A., Zelenyuk, A., and Zhang, Q.: Recent advances in
1098 understanding secondary organic aerosol: Implications for global climate forcing, *Rev.*
1099 *Geophys.*, 55, 509–559, 2017.

1100 Shrivastava, M., Fast, J., Easter, R., Gustafson, W. I., Zaveri, R. A., Jimenez, J. L., Saide, P.,
1101 and Hodzic, A.: Modeling organic aerosols in a megacity: comparison of simple and
1102 complex representations of the volatility basis set approach, *Atmos. Chem. Phys.*, 11,
1103 6639–6662, 2011.

1104 Sun, Y., Jiang, Q., Wang, Z., Fu, P., Li, J., Yang, T., and Yin, Y.: Investigation of the sources and
1105 evolution processes of severe haze pollution in Beijing in January 2013, *J. Geophys. Res.,*
1106 *Atmos.*, 119, 4380–4398, 2014.

1107 Tang, J., Li, Y., Li, X., Jing, S., Huang, C., Zhu, J., Hu, Q., Wang, H., Lu, J., Lou, S., Rao, P.,
1108 and Huang, D.: Intermediate volatile organic compounds emissions from vehicles under
1109 real world conditions, *Sci. Total Environ.*, 788, 147795, 2021.

1110 Tao, J., Zhang, L., Cao, J., and Zhang, R.: A review of current knowledge concerning PM_{2.5}
1111 chemical composition, aerosol optical properties and their relationships across China,
1112 *Atmos. Chem. Phys.*, 17, 9485–9518, 2017.

1113 Tkacik, D. S., Presto, A. A., Donahue, N. M., and Robinson, A. L.: Secondary organic aerosol
1114 formation from intermediate-volatility organic compounds: Cyclic, linear, and branched
1115 alkanes, *Environ. Sci. Technol.*, 46, 8773–8781, 2012.

1116 Tsimpidi, A. P., Karydis, V. A., Zavala, M., Lei, W., Molina, L., Ulbrich, I. M., Jimenez, J. L.,
1117 and Pandis, S. N.: Evaluation of the volatility basis-set approach for the simulation of
1118 organic aerosol formation in the Mexico City metropolitan area, *Atmos. Chem. Phys.*, 10,
1119 525–546, 2010.

1120 US EPA: Final Report, SPECIATE Version 5.1, Database Development Documentation,
1121 available at: [https://www.epa.gov/air-emissions-modeling/speciate-51-and-50-addendum-](https://www.epa.gov/air-emissions-modeling/speciate-51-and-50-addendum-and-final-report)
1122 [and-final-report](https://www.epa.gov/air-emissions-modeling/speciate-51-and-50-addendum-and-final-report) (last access: 8 August 2021), 2021

1123 Woody, M. C., Baker, K. R., Hayes, P. L., Jimenez, J. L., Koo, B., and Pye, H. O. T.:
1124 Understanding sources of organic aerosol during CalNex-2010 using the CMAQ-VBS,
1125 *Atmos. Chem. Phys.*, 16, 4081–4100, 2016.

1126 Wu, L., Ling, Z., Liu, H., Shao, M., Lu, S., Wu, L., and Wang, X.: A gridded emission inventory
1127 of semi-volatile and intermediate volatility organic compounds in China, *Sci. Total*
1128 *Environ.*, 761, 143295, 2021.

1129 Wu, L., Wang, X., Lu, S., Shao, M., and Ling, Z.: Emission inventory of semi-volatile and
1130 intermediate-volatility organic compounds and their effects on secondary organic aerosol
1131 over the Pearl River Delta region, *Atmos. Chem. Phys.*, 19, 8141–8161, 2019.

1132 Xu, L., Guo, H., Boyd, C. M., Klein, M., Bougiatioti, A., Cerully, K. M., Hite, J. R., Isaacman-
1133 VanWertze, G., Kreisberg, N. M., Knote, C., Olson, K., Koss, A., Goldstein, A. H., Hering,
1134 S. V., de Gouw, J., Baumann, K., Lee, S., Nenes, A., Weber, R. J., and Ng, N. L.: Effects
1135 of anthropogenic emissions on aerosol formation from isoprene and monoterpenes in the
1136 southeastern United States, *P. Natl. Acad. Sci. USA*, 112, 37–42, 2015.

1137 Yang, W., Li, J., Wang, W., Li, J., Ge, M., Sun, Y., Chen, X., Ge, B., Tong, S., Wang, Q., and
1138 Wang, Z.: Investigating secondary organic aerosol formation pathways in China during
1139 2014, *Atmos. Environ.*, 213, 133–147, 2019.

1140 Yao, T., Li, Y., Gao, J., Fung, J. C. H., Wang, S., Li, Y., Chan, C. K., and Lau, A. K. H.: Source
1141 apportionment of secondary organic aerosols in the Pearl River Delta region: Contribution
1142 from the oxidation of semi-volatile and intermediate volatility primary organic aerosols,
1143 *Atmos. Environ.*, 222, 117111, 2020.

1144 Yu, K., Zhu, Q., Du, K., and Huang, X.: Characterization of nighttime formation of particulate
1145 organic nitrates based on high-resolution aerosol mass spectrometry in an urban
1146 atmosphere in China, *Atmos. Chem. Phys.*, 19, 5235–5249, 2019.

1147 Yuan, B., Shao, M., Lu, S., and Wang, B.: Source profiles of volatile organic compounds
1148 associated with solvent use in Beijing, China, *Atmos. Environ.*, 44, 1919–1926, 2010.

1149 Zhang, H., Yee, L. D., Lee, B. H., Curtis, M. P., Worton, D. R., Isaacman-VanWertz, G.,
1150 Offenberg, J. H., Lewandowski, M., Kleindienst, T. E., Beaver, M. R., Holder, A. L.,
1151 Lonneman, W. A., Docherty, K. S., Jaoui, M., Pye, H. T. O., Hu, W., Day, D. A.,
1152 Campuzano-Jost, P., Jimenez, J. L., Guo, H., Weber, R. J., de Gouw, J., Koss, A. R.,
1153 Edgerton, E. S., Brune, W., Mohr, C., Lopez-Hilfiker, F. D., Lutz, A., Kreisberg, N. M.,
1154 Spielman, S. R., Hering, S. V., Wilson, K. R., Thornton, J. A., and Goldstein, A. H.:
1155 Monoterpenes are the largest source of summertime organic aerosol in the southeastern
1156 United States, *P. Natl. Acad. Sci. USA*, 115, 2038–2043, 2018.

1157 Zhang, Q., Jimenez, J. L., Canagaratna, M. R., Allan, J. D., Coe, H., Ulbrich, I., Alfarra, M. R.,
1158 Takami, A., Middlebrook, A. M., Sun, Y. L., Dzepina, K., Dunlea, E., Docherty, K.,
1159 DeCarlo, P. F., Salcedo, D., Onasch, T., Jayne, J. T., Miyoshi, T., Shimono, A., Hatakeyama,

1160 S., Takegawa, N., Kondo, Y., Schneider, J., Drewnick, F., Borrmann, S., Weimer, S.,
1161 Demerjian, K., Williams, P., Bower, K., Bahreini, R., Cottrell, L., Griffin, R. J., Rautiainen,
1162 J., Sun, J. Y., Zhang, Y. M., and Worsnop, D. R.: Ubiquity and dominance of oxygenated
1163 species in organic aerosols in anthropogenically-influenced Northern Hemisphere
1164 midlatitudes, *Geophys. Res. Lett.*, 34, L13801, 2007.

1165 Zhang, Q., Jimenez, J. L., Canagaratna, M. R., Ulbrich, I. M., Ng, N. L., Worsnop, D. R., and
1166 Sun, Y.: Understanding atmospheric organic aerosols via factor analysis of aerosol mass
1167 spectrometry: a review, *Anal. Bioanal. Chem.*, 401, 3045–3067, 2011.

1168 Zhang, Y., Vijayaraghavan, K., and Seigneur, C.: Evaluation of three probing techniques in a
1169 three-dimensional air quality model, *J. Geophys. Res., Atmos.*, 110, D02305, 2005.

1170 Zhao, B., Wang, S., Donahue, N. M., Jathar, S. H., Huang, X. F., Wu, W., Hao, J., and Robinson,
1171 A. L.: Quantifying the effect of organic aerosol aging and intermediate-volatility emissions
1172 on regional scale aerosol pollution in China, *Sci. Rep.*, 6, 28815, 2016a.

1173 Zhao, Y., Hennigan, C. J., May, A. A., Tkacik, D. S., De Gouw, J. A., Gilman, J. B., Kuster, W.
1174 C., Borbon, A., and Robinson, A. L.: Intermediate-volatility organic compounds: A large
1175 source of secondary organic aerosol, *Environ. Sci. Technol.*, 48, 13743–13750, 2014.

1176 Zhao, Y., Kreisberg, N. M., Worton, D. R., Isaacman, G., Weber, R. J., Liu, S., Day, D. A.,
1177 Russell, L. M., Markovic, M. Z., VandenBoer, T. C., Murphy, J. G., Hering, S. V., and
1178 Goldstein, A. H.: Insights into secondary organic aerosol formation mechanisms from
1179 measured gas/particle partitioning of specific organic tracer compounds, *Environ. Sci.*
1180 *Technol.*, 47, 3781–3787, 2013.

1181 Zhao, Y., Nguyen, N. T., Presto, A. A., Hennigan, C. J., May, A. A., and Robinson, A. L.:
1182 Intermediate volatility organic compound emissions from on-road diesel vehicles:
1183 Chemical composition, emission factors, and estimated secondary organic aerosol
1184 production, *Environ. Sci. Technol.*, 49, 11516–11526, 2015.

1185 Zhao, Y., Nguyen, N. T., Presto, A. A., Hennigan, C. J., May, A. A., and Robinson, A. L.:
1186 Intermediate Volatility Organic Compound Emissions from On-Road Gasoline Vehicles
1187 and Small Off-Road Gasoline Engines, *Environ. Sci. Technol.*, 50, 4554–4563, 2016b.

1188 Zheng, M., Cass, G. R., Schauer, J. J., and Edgerton, E. S.: Source Apportionment of PM_{2.5} in
1189 the Southeastern United States Using Solvent-Extractable Organic Compounds as Tracers,
1190 Environ. Sci. Technol., 36, 2361–2371, 2002.

1191 Zhu, S., Wang, Q., Qiao, L., Zhou, M., Wang, S., Lou, S., Huang, D., Wang, Q., Jing, S., Wang,
1192 H., Chen, C., Huang, C., and Yu, J. Z.: Tracer-based characterization of source variations
1193 of PM_{2.5} and organic carbon in Shanghai influenced by the COVID-19 lockdown, Faraday
1194 Discuss., 226, 112, 2021.

1195 Zhu, W., Zhou, M., Cheng, Z., Yan, N., Huang, C., Qiao, L., Wang, H., Liu, Y., Lou, S., and
1196 Guo, S.: Seasonal variation of aerosol compositions in Shanghai, China: Insights from
1197 particle aerosol mass spectrometer observations, Sci. Total Environ., 771, 144948, 2021.

1198